An-Najah National University

Faculty of Graduate Studies

RASHBA AND DRESSELHAUS SPIN ORBIT EFFECTS ON THE MAGNETIZATION AND MAGNETIC SUSCEPTIBILITY OF INAS-QUANTUM WIRE

By

Wafa Haj Mohammad

Supervisors

Prof. Mohammad Elsaid

Dr. Maen Ishtawi

This Thesis is submitted in Partial Fulfillment of the Requirements for the Degree of Master of Physics, Faculty of Graduate Studies, An-Najah National University, Nablus, Palestine.

2022

Dedication

My mother and father, whose no words enough to thank them, whose gave me a sincere heart believes that there is no impossible.

My deepest gratitude to my Uncle (**Mahmoud Haj Mohammed**), who gives me the support, hope and care during my Bachelor and master study.

To my Uncle (**Abdulrahim Asrawi**), who gives me the hope and support during my master study.

My wonderful and dearest husband **(Issa)**, who is sharing with me every moment and gave me trust and belie in everything I do, encouraged me all the time.

My kind and sweet son **(Abdulrahim)**.

My Brothers: **(Ibraheem, Ahmad, Shima & Salma)**.

Acknowledgments

All thanks goes Allah, who gives me the power and the health to complete my thesis.

I would like to thank my supervisor Prof. Mohammad Elsaid and my co-supervisor Dr. Maen Ishtawi for their assistance, efforts and guidance. Mr. Ayham Shaer who helps me to use Mathematica program.

I cannot forget to thank An-Najah National University and the members of the physics department.

Declaration

I, the undersigned, declare that I submitted the thesis entitled:

RASHBA AND DRESSELHAUS SPIN ORBIT EFFECTS ON THE MAGNETIZATION AND MAGNETIC SUSCEPTIBILITY OF INAS- QUANTUM WIRE

I declare that the work provided in this thesis, unless otherwise referenced, is the researcher's own work, and has not been submitted elsewhere for any other degree or qualification.

Student's Name: Wafa Haj Mohammad

Signature:

Date: 25/09/2022

Table of Contents

List of Tables

List of Figures

RASHBA AND DRESSELHAUS SPIN ORBIT EFFECTS ON THE MAGNETIZATION AND MAGNETIC SUSCEPTIBILITY OF INAS- QUANTUM WIRE

By
Wafa Haj Mohammad
Supervisors
Prof. Mohammad El-Said
Dr. Maen Ishtaiwi

Abstract

Background: Nanomaterials play an important role in our life due to their potential in a wide range of device applications. Nano-materials are classified, according to their dimensions, into four types: Bulk, quantum well (QW), quantum well wire (QWW) and quantum dot (QD). A lot of research has been conducted on the properties of InAs QW and QWW material in the presence of an electric field. This study has looked at the magnetic properties of InAS QWW material under Rashba, Dresselhaus and the magnetic field effects. Transverse confinement potential was also taken into account.

Methodology: Magnetic properties, like magnetization and susceptibility for InAs quantum well wire (QWW) material, have been studied theoretically under applied external magnetic field, with spin orbital interactions (SOI) like Rashba and Dresselhaus effects. The Hamiltonian of a single electron, confined in a QWW, has been solved by exact diagonalization method to obtain the eigenvalues and eigenfunctions of energy states as a function of QWW physical parameters. The researcher computed the average energy and the eigenstates of energy sub-bands that split under external magnetic field, using Rashba effect and Dresselhaus effect. Magnetization and susceptibility were studied and the oscillating behavior of the curves were observed as a result of mixing energy sub-bands of QWW spectra.

Transverse conferment potential was taken into account. The average energy was studied under three effects with an external magnetic field. The magnetic properties were studied as well.

Results: The calculations showed clearly that the Rashba parameter was an important and effective factor in controlling the magnetic properties of QWW material type. Dresselhaus parameter was also an effective factor but was weaker than Rashba effect. The Transverse confinement potential had a marginal effect on magnetic properties of InAs-QWW material. However, the temperature showed a significant effect on the magnetic properties of the conceded QWW. When T increased, the average energy would increase, too. Therefore, magnetization M and susceptibility χ behaviors would accordingly change.

Conclusion: Rashba parameter is an important and effective factor that can control the magnetic properties of InAs QWW material. Dresselhaus parameter can also control the magnetic properties, but it is weaker than Rashba parameter. The Transverse confining potential has a marginal effect on magnetization and susceptibility of InAs-QWW material.

Keywords: InAs QWW, Rashba, Dresselhaus, magnetic field, magnetization, susceptibility.

Chapter One
Introduction

1.1 The Nano system

The utilization of matter on an atomic, molecular, and supramolecular scale for industrial purposes is known as nanotechnology, or just nanotech. The initial and most popular definition of nanotechnology, currently known as molecular nanotechnology, focused on the specific technological objective of accurately manipulating atoms and molecules for the creation of macroscale objects. The National Nanotechnology Initiative has since developed a broader definition of nanotechnology.

Nano system is scale of structure which deals with small structure of materials, which have a scale about 1-100 nanometer[1]. Figure. 1.1 shows different atoms that have 1nm dimensions.

This definition changed from a specific technological goal to a research category inclusive of all types of research and technologies that deal with the unique properties of matter that occur below the specified size threshold in order to reflect the importance of quantum mechanical effects at this quantum-realm scale. As a result, the term "nanotechnologies" or "nanoscale technologies" is frequently used to refer to a wide range of research and applications that share the characteristic of being small.

A size-based definition of nanotechnology encompasses a variety of scientific disciplines, including surface science, organic chemistry, molecular biology, semiconductor physics, energy storage, engineering, microfabrication, and molecular engineering. The related research and applications include a wide range of topics, from modifications of traditional device physics to entirely novel strategies based on molecular self-assembly, from creating novel materials with nanoscale dimensions to precise control of matter at the atomic level.

Scientists are currently debating how nanotechnology will affect society in the future. Nanotechnology may be able to develop a wide variety of new products, including consumer goods, nanomedicine, nanoelectronics, biomaterials, and energy production. On the other hand, nanotechnology raises many of the same problems as any new technology,

such as worries about the toxicity and environmental impact of nanomaterials, as well as their potential to have an impact on the world's economies and the speculative possibility of various doomsday scenarios. These worries have sparked a discussion about the need for special regulation of nanotechnology among advocacy groups and governments.

Figure 1.1

Different Atoms Showing Dimensions of 1 nm When Aligned in a Row[2].

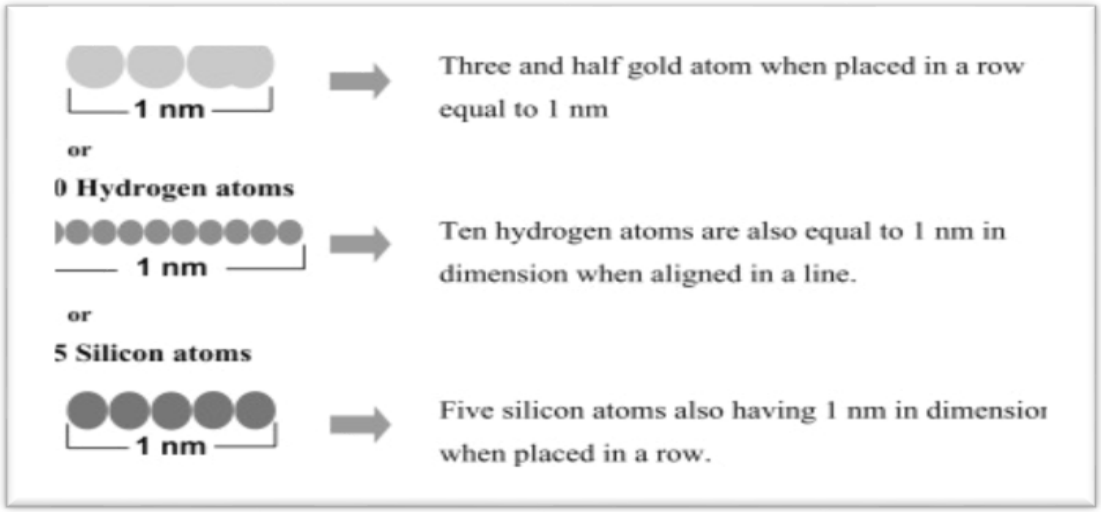

The field of nanomaterials encompasses subfields that create or research materials with particular features brought on by their nanoscale dimensions. Many materials that may be beneficial in nanotechnology, including carbon nanotubes and other fullerenes, as well as other nanoparticles and nanorods, have been developed thanks to interface and colloid science. Nanoionics and nanoelectronics are also connected to nanomaterials with rapid ion transport.

The majority of current commercial applications of nanotechnology are of this type, and nanoscale materials can also be used for bulk applications. Many materials that may be beneficial in nanotechnology, including carbon nanotubes and other fullerenes, as well as other nanoparticles and nanorods, have been developed thanks to interface and colloid science. Nanoionics and nanoelectronics are also connected to nanomaterials with rapid ion transport.

The majority of current commercial applications of nanotechnology are of this type, although nanoscale materials can also be used for bulk applications. Utilizing these materials for medical purposes has advanced; see Nanomedicine. In order to reduce the

cost of conventional silicon solar cells, nanoscale materials like nanopillars are occasionally employed in solar cells. development of semiconductor nanoparticle-based products for use in the upcoming generation of goods, including displays, lighting, solar cells, and biological imaging; see quantum dots.

A variety of biomedical applications, such as tissue engineering, drug delivery, antibacterial, and biosensors, have recently used nanomaterials.

Nanomaterials play an important role due to their potential in a wide range of device applications. The nanodevices have a novel characteristic since they have smaller and faster technical machines. Properties of low-dimensional nanostructures, such as, electronic, magnetic, thermodynamic and optical properties are of the most interest to nanoscience community. Nanoscience is the study and applications of the small things that can be used in many science fields, such as, biology, chemistry, medicine, material science, and engineering. Materials in the micrometer scale mostly exhibit physical properties similar to that of the bulk form. However, materials in the nanometer scale may exhibit physical properties distinctively different from that of bulk form. Any material in this size range exhibits remarkable specific properties, such as a transition from atoms or molecules to bulk form. The effect of reduction dimensionality for semiconductors produced by confining of the motion of charge carriers i.e., the holes and the electrons in one, two or three directions that affects the on physical properties of the material such that electrical, chemical and optical properties **[3].**

The dimensionality refers to the number of degrees of freedom for the momentum carriers or electrons. So, the nanomaterials are classified into four types according to these dimensions and those types are: Bulk, quantum well (QW), quantum well wire (QWW) and quantum dot (QD).

Assume that the number of degrees of freedom is D_f and the number of confinement directions is D_c, then for all types of materials $D_f + D_c = 3$[4].

Table 1.1 shows the types of materials according to the quantum confining structure.

Table 1.1

Classification of quantum confined structures.

Type	D_f	D_c
Bulk	3	0
QW	2	1
QWW	1	2
QD	0	3

The change of dimension of motion of the electrons leads to change the amount of energy bands for the bulk. Its changes from continues energy band gap to discrete and the absorption spectrum become discrete.

A potential well with only discrete energy values is referred to as a quantum well.

In the traditional approach, particles that were previously free to move in three dimensions are constrained to only move in two dimensions by being made to occupy a planar space. When the quantum well thickness reaches a point where it is comparable to the de Broglie wavelength of the carriers, which are typically electrons and holes, quantum confinement takes effect, creating energy levels known as "energy sub-bands," meaning that the carriers can only have discrete energy values. Based on the principle of quantum well systems, a wide range of electronic quantum well devices have been created. For instance, these gadgets are used in switches, modulators, photodetectors, and lasers. Quantum well devices are incredibly important to the technology and telecommunications industries because they work considerably more efficiently and quickly than traditional devices. The majority, if not all, of the conventional electrical components in many electronic devices are currently being replaced by these quantum well devices. The idea of a quantum well was independently put forth in 1963 by Herbert Kroemer, Zhores Alferov, and R.F. Kazarinov.

The comprehensive theoretical and computational information needed to comprehend the electrical, optical, and transport properties of these semiconductor nanostructures is provided in Quantum Wells, Wires, and Dots. Through thorough explanations and mathematical derivations, the book will guide the reader to the point where they may develop semiconductor nanostructures with the necessary electrical and optical properties for use in these technologies.

This fourth edition's new parts, which make heavy use of contemporary technology, and updated content include:

1. Non-parabolic energy bands' characteristics
2. Poisson and Schrödinger equations' matrix solutions
3. Minimum stressed material thickness
4. Carrier scattering by alloy disorder, interface roughness, and contaminants
5. Modeling of density matrix transport
6. Thermal simulation

This user-friendly manual, written by renowned experts in the fields of semiconductor nanostructures and quantum optoelectronics, is presented in a clear manner with easy-to-follow steps, illustrative examples and questions, and computational problems in each chapter to help the reader build strong conceptual foundations so they can start their own theoretical investigations. The book is crucial for everyone conducting research in academic and commercial laboratories around the world. It is appropriate for postgraduate students of semiconductor and condensed matter physics.

To get solutions to the issues, instructors can get in touch with the authors directly.

If we compare the density of states for the bulk structure with QW then, we find that the QW has higher density of states near the edges of the conduction and valance bands that mean more carriers of energy concentration can contribute to the band- edge emission[5].

Moreover, for more confined dimensions, there will be more discrete energy levels as shown in Figure 1.2. for bulk, QW, QWW and QD.

The optical and electrical characteristics of quantum dots (QDs), which are semiconductor particles a few nanometers in size, differ from those of bigger particles due to the laws of quantum mechanics. They play a significant role in nanotechnology. An electron inside a quantum dot can be stimulated to a higher energy level when it is exposed to UV radiation. This mechanism corresponds to an electron moving from the valence band to the conductance band in a semiconducting quantum dot. When the excited electron returns to the valence band, it can emit light and release its energy. The image on the right demonstrates this light emission (photoluminescence).The energy difference between the

conductance band and the valence band, or the transition between discrete energy levels when band structure is no longer a useful concept in QDs, determines the hue of that light.

Nanoscale semiconductor materials tightly restrict either electrons or electron holes, to use the vocabulary of materials science. In order to emphasize their uniqueness and the fact that they have constrained, discrete electronic states, just like naturally occurring atoms or molecules, quantum dots are sometimes referred to as artificial atoms. It was established that the electronic wave functions in quantum dots are comparable to those in actual atoms. One can create an artificial molecule that exhibits hybridization even at room temperature by coupling two or more of these quantum dots. Between discrete atoms or molecules and bulk semiconductors, quantum dots have characteristics in the middle. Their optoelectronic characteristics vary with both their size and shape. Longer wavelengths are emitted by larger QDs with a diameter of 5–6 nm. These colors include orange or red. Shorter wavelengths are emitted by smaller QDs (2–3 nm), producing colors like blue and green. The precise makeup of the QD affects the specific hues, though. Quantum dots have the potential to be used in single-electron transistors, solar cells, LEDs, lasers, single-photon sources, second-harmonic generation, quantum computing, microscopy, medical imaging, and more. Some QDs can be suspended in solutions due to their small size, which may enable their usage in spin-coating and inkjet printing. They were utilized in Langmuir-Blodgett thin films . These processing approaches produce semiconductor production processes that are less expensive and time-consuming[6].

Figure 1.2

Charge carriers are confined in a semiconductor (red) with a smaller bandgap than the cladding semiconductor (blue). The confinement changes the density of states D(E). Ec is the conduction-band edge of a 3D semiconductor[7].

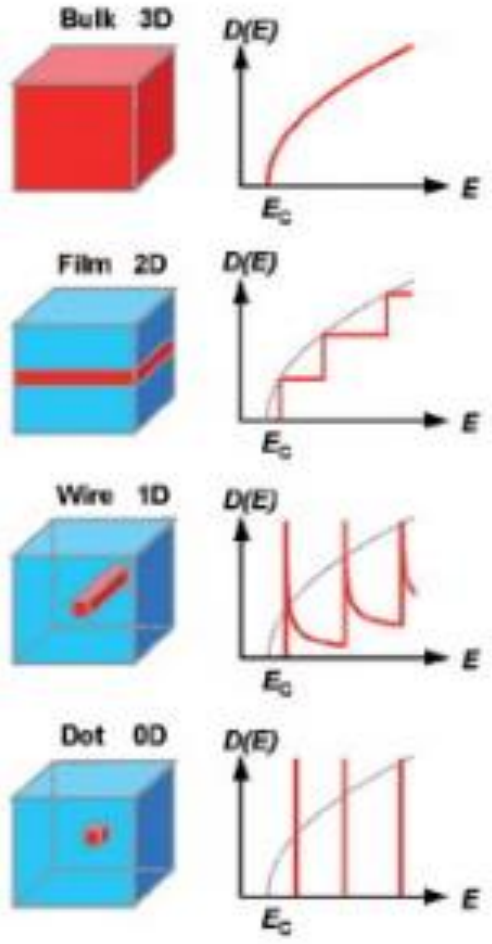

1.2 Spintronics

Spintronics, or spin electronics "is an emerging field of nanoscale electronics involving both the **charge** and **spin** of an electron. Spintronics used to carry an excitement information for its potential in a wide range of applications"[8].

Spintronics is another name for spin Flextronics is the study of fundamental electrical charge in solid-state devices, as well as the inherent spin of the electrons and its magnetic moment. For instance, significant solid-state physics problems like spin transport and spin relaxation in semiconductors and metals are included in fundamental research together with new technology being used in electronic storage technology.

Spin-dependent electron transport processes in solid-state devices were discovered in the 1980s, and this led to the development of spintronics. This includes the finding of enormous magnetoresistance separately by Albert Fert et al. and Peter Grünberg et al., as well as the observation of spin-polarized electron injection from a ferromagnetic metal to a nonmagnetic metal by Johnson and Silsbee (1985). (1988). The ferromagnet/superconductor tunneling experiments, which Meservey and Tedrow pioneered, as well as Julliere's early research on magnetic tunnel junctions, were the forerunners of spintronics. The theoretical development of a spin field-effect transistor by Datta and Das in 1990 and the electric dipole spin resonance by Rashba in 1960 marked the beginning of the usage of semiconductors for spintronics[9].

We study the spintronics to understand and to find effective ways to control the electronic properties such as accumulated charge or the current by magnetic field or spin, controlling of the magnetic properties or the spin by a gate voltage or by an electric field. In addition we want to understand the main concept of spin transport and the interaction between the interaction spin and its environments **[10].**

The elementary charge of electrons used in electronic devices in its transport. The controllable switch occurred when we apply a voltage to the semiconductor so, the electrical conductivity can be tuned. These switches are the main idea for building blocks of implementation for hardware logic. Electron carries charge and also it carries spin or angular momentum. The Stern-Gerlach experiment demonstrated that the special orientation of angular momentum is quantized. That means the spin of electron can only be up or down and that depend on the measurement apparatus[11]. The direction of the spin (up or down) similar to the "0" and "1" digital states thus can be used to represent the binary memory states. Spintronics is a new research area, which deals with controlling the spin direction of the carriers inside materials [12]. We need to use the spintronics to satisfy the requirement of fast response, large capacity and small size. The new spintronics devices mixed between the logic, sensor applications and storage. These devices lead us to manufacture a new computer that have quantum computation ability that is based on electric solid-state devices.

There is a lot of research being done on non-volatile spin-logic devices to facilitate scaling. Devices with spin-transfer, torque-based logic that process information by using

spins and magnets have been proposed. The exploratory road map for the ITRS includes these devices. Applications for logic-in-memory are already under development. Materials Today has an article from 2017 that reviews the year.

In order for SPICE researchers and later circuit and system designers to use the physics of spin transport for the exploration of spintronics for "beyond CMOS computing," a generalized circuit theory for spintronic integrated circuits has been presented[ ] .

Reduced ferromagnetism is visible in doped semiconductor materials. Dilute magnetic oxides (DMOs), such as those based on ZnO and TiO2, have been the focus of a great deal of experimental and computational research in recent years. In order to boost the interface resistance, non-oxide ferromagnetic semiconductor sources, such as manganese-doped gallium arsenide (Ga,Mn)As, can either use a tunnel barrier or hot electron injection.

Various methods have been used to detect spin in semiconductors:

1. Transmitted/reflected photon rotation according to Faraday and Kerr
2. Electroluminescence circular polarization analysis
3. Nonlocal spin valve (derived from studies with metals by Johnson and Silsbee)
4. Filtering for ballistic spin

The latter method was utilized to establish spin transport in silicon despite the material's limitations and the lack of spin-orbit interaction.

Due to the fact that strong Hall effects and magnetoresistance in semiconductors can be produced by external magnetic fields (also by stray fields from magnetic contacts), the Hanle effect, which shows spin precession and dephasing in a magnetic field that is not collinear to the injected spin orientation, is the sole definitive proof of spin transport in semiconductors[10].

The output of circularly polarized coherent light can be controlled in applications using spin-polarized electrical injection. Lasers made of semiconductors are an example. A spin-based transistor with advantages over MOSFET devices, such as a steeper sub-threshold slope, may find use in the future.

Magnetic tunnel transistor: A single base layer magnetic tunnel transistor includes the following terminals:

a. Spin-polarized hot electrons are introduced into the base by emitter (FM1).
b. Base (FM2): The base experiences spin-dependent scattering. In addition, it works as a spin filter.
c. A Schottky barrier forms at the interface, collector (GaAs). Only electrons with enough energy to break through the Schottky barrier and when semiconductor states are available are collected[9].

Since antiferromagnetic material may store bits just as well as ferromagnetic material, antiferromagnetic storage media have been investigated as an alternative to ferromagnetism. The states can be, for example, 0 "vertically-alternating spin configuration" and 1 "horizontally-alternating spin configuration" instead of the conventional definition 0 "magnetization upwards" and 1 "magnetization downwards".

The following are the key benefits of antiferromagnetic material:

1. Zero net external magnetization renders antiferromagnetic device elements insensitive to data-damaging perturbations by stray fields
2. No impact on nearby particles
3. Significantly shorter switching times (antiferromagnetic resonance frequency is in the THz range compared to GHz ferromagnetic resonance frequency)
4. A wide variety of commercially available antiferromagnetic materials including insulators, sems, and semiconductors.

Antiferromagnetic spintronics' net zero magnetism makes reading and writing information to them more challenging than to ferromagnetic spintronics, hence research is being done in this area. In modern MRAM, reading and writing by electrical current, which is more effective and scalable, has largely replaced the detection and manipulation of ferromagnetic order by magnetic fields. Antiferromagnets are also being studied for ways to read and write information using current rather than fields because fields are useless in antiferromagnets. Antiferromagnets are now being studied for writing techniques using spin-transfer torque, spin-orbit torque, and the Rashba effect. It is also being investigated to read information from antiferromagnets via magnetoresistance effects like tunnel magnetoresistance[10].

The giant-magneto resistive (GMR) sandwich structure, which is made of alternating ferromagnetic and non-magnetic metal layers, was developed with the aid of spintronics. This device is utilized in industry as a read head and a memory-storage cell. The device resistance varies from tiny (parallel magnetizations) to large (perpendicular magnetizations) depending on the relative orientation of the magnetizations in the magnetic layers (antiparallel magnetizations).

Magnetic field changes can be detected using this change in resistance, also known as magnetoresistance. The magnetic field of an electron can be described as having one of two positions, known as up or down. The traditional high and low logic values, which are represented by simple currents, are given an additional two binary states as a result. A bit can exist in four different states when the spin state is included. These states are up-high, up-low, down-high, and down-low. Quantum bits, or qubits, are represented by these four states.

1.3 Rashba Spin-orbit interaction

Spin orbit interaction (SOI) is the coupling between spin electron dynamics and its orbital motion in space. Based on special relativity theory, magnetic and electric fields are Lorentz transformed when changing the reference of inertial frame[13] [14]. Therefore, when an electron moves through an electric filed it is seen in its rest frame as moving charges, i.e., electric filed. While these moving charges are seen as an internal magnetic field in the rest frame of the electron itself[15]. The velocity and travel direction of the election in material specify the direction and the magnitude of the internal magnetic field, i.e., SOI gives rise to a k-dependent internal magnetic field, where k is the wave vector of the electron. Utilizing the coupling between electron spin and its orbital motion is one of the major tools to control magnetism in spintronics. Spin momentum locking is the process of inducing magnetic textures of band electrons by Rashba and Dresselhaus spin-orbit couplings[16].

Rashba SOI effect generates from confining the motion of electrons into a thin two dimensional electron gas (2DEG) layer by an asymmetric confinement potential which leads to couple the degrees of freedom of these electrons. The importance of this mechanism lies in the fact that the asymmetry in the confinement potential can be varied by electrostatic means, allowing to tune the SOI strength by an external gate voltage[17].

The Hamiltonian of Rashba SOI is:

$$\widehat{H_R} = \alpha_R \left(\hat{P} \times \sigma\right).\hat{Z} \tag{1.1}$$

Where α_R is the Rashba spin-orbital coupling parameter which can be varied by the gate electric field, $\hat{P}$ is the momentum operator, $\boldsymbol{\sigma}$ is a vector of Pauli matrices, and $\hat{Z}$ the direction of the effect of the asymmetric confinement potential on the InAs QWW.

The total Hamiltonian of electron due to the Rashba effect is given by

$$\hat{H} = \widehat{H_0} + \widehat{H_R} \tag{1.2}$$

Where ($\widehat{H_0} = \frac{\hbar^2 K^2}{2\,m}$) is Hamiltonian of the free electron. Diagonalizing this Hamiltonian yields the following energy spectrum:

$$E_n\,(k) = \frac{\hbar^2 k^2}{2m} \pm \alpha_R\,|\vec{K}| \tag{1.3}$$

Where; $E_n\,(k)$ is eigen value of energy, α_R is called Rashba parameter and $\vec{\boldsymbol{K}}$ is wave vector**.**

Spin and Orbital Rashba Effects:

The spin-orbit interaction in quantum physics is a relativistic interaction between a particle's spin and its motion inside a potential. It is also known as the spin-orbit effect or spin-orbit coupling. The electromagnetic interaction between an electron's magnetic dipole, orbital motion, and the electrostatic field of the positively charged nucleus causes changes in an electron's atomic energy levels, which is a key example of this phenomena. This phenomena can be observed as a splitting of spectral lines, which is a Zeeman effect produced by two relativistic effects: the magnetic moment of the electron connected to its intrinsic spin and the apparent magnetic field as seen from the perspective of the electron. Due to the connection between angular momentum and the strong relationship between Protons and neutrons traveling within the nucleus experience the nuclear force, which causes a change in their energy levels according to the nucleus shell model. Spin-orbit effects for electrons in semiconductors and other materials are investigated for practical applications in the subject of spintronics. The spin Hall

effect and magneto crystalline anisotropy are both products of the spin-orbit interaction.

When it comes to atoms, the amount of the energy level splitting caused by the spin-orbit interaction is often on par with the relativistic corrections to kinetic energy and the zitterbewegung effect. The fine structure is the culmination of these three modifications. The energy levels are slightly corrected by the interaction of the magnetic field produced by the electron with the magnetic moment of the nucleus the hyperfine structure is so called.

In crystals the inversion symmetry broken, the SOC split the electronic states. The Rashba SOC generated due to the interaction between the electron's spin σ and the momentum of crystal K

$$H_{SO} = \alpha_R(\sigma\, x\, K).\hat{Z}$$

Where is:

α_R: Rashba parameter

$\hat{Z}$: the unit vector along in which the inversion symmetry is broken.

The Rashba SOC produces a chiral spin angular momentum space because of the spin-momentum coupling. The Hamiltonian of 2D free electron with Rashba SOC

$$H = \frac{k^2}{2m} + \alpha_R(\sigma \times \boldsymbol{K}).\hat{z}$$

Where is $k = \sqrt{k_x^2 + k_y^2}$.

By derive the eigenvalue equation $H|\Psi> = E\,|\Psi>$, one obtains the Dirac cone-like energy splitting with original parabolic dispersion,

$$E_{\pm}(k) = \frac{k^2}{2m} \pm \alpha_R\, k$$

The Rashba SOC is different from the Zeeman splitting because it shifts the two degenerate bands along the momentum axis. The corresponding eigenstates are

$$\left|\begin{array}{l}\Psi_{+}(K)>=\frac{1}{\sqrt{2}}\left(|\uparrow>-i\,e^{i\theta_k}|\downarrow>\right)|-\Psi(K)> \\ \qquad\quad=\frac{1}{\sqrt{2}}\left(-ie^{-i\theta_k}|\uparrow>+|\downarrow>\right)\end{array}\right|$$

where $|\uparrow> and |\downarrow>$ are the spin- up and spin-down states with respect to the z-direction respectively.

θ_k : is the angle of the momentum defined by

$$k = (\cos(\theta_k), Sin(\theta_k))$$

The spin structure is obtained by the expectation value

$$< \Psi_{\pm}(K)|\sigma|\Psi_{\pm}(K) >= \pm(\frac{K_y}{K}, -\frac{K_x}{K})$$

Spin-orbit (SO) coupling divides electronic energy bands in crystals without an inversion center. For no centrosymmetric wurtzite semiconductors, the Rashba SO coupling was initially proposed, a SO coupling linear in momentum p. Bychkov and Rashba employed modulation-doped semiconductor heterostructures to the SO coupling in a two-dimensional electron gas (2DEG) with structural inversion asymmetry after their development. The simplest two-dimensional free electron approximation decreases to a linear dependence when SO coupling approaches odd in momentum p in systems with inversion symmetry breakdown. Numerous materials without spatial inversion have odd-in-p SO coupling proven in them. The fundamental characteristic of any SO coupling is the phenomenon that electrons travelling in an electric field encounter.

1.4 Dresselhaus Effect

Promising prospects to investigate electron topological transitions are two-dimensional electron systems with integrated Rashba and Dresselhaus spin orbit interaction (SOI), which have a complex energy spectrum with a conical point and four critical points.

A phenomenon in solid state physics in which SOI causes energy bands to split and it's usually present in crystal systems lacking inversion symmetry. This phenomenon is known as Dresselhaus effect[18].

As its known, spin-orbital coupling is a relativistic interaction between the dipole moment produced by the relative motion of the electron and the resulting electric filed from an ion-core. In atoms, this coupling causes weakly split of energy states into two states. One of them with anti-aligned spin to the orbital field and the other with aligned spin.

Due to the coupling between the electron spin and the lattice potential in solid crystalline material, the motion of the conduction electrons altered by a complementary effect in the lattice. The asymmetry in the potential can favor one spin orientation over the opposite and split the energy bands into spin aligned and anti-aligned sub-bands.

The Dresselhaus spin-orbital Hamiltonian can be approximated as,

$$\widehat{H_D} = \frac{\beta_D}{\hbar}\,\widehat{p_z^2}\left[\,\sigma_y\left(\widehat{p_y} + e\,B_x\right) - \sigma_x\,\widehat{p_x}\,\right] \tag{1.4}$$

Where $\boldsymbol{\beta_D}$ is the Dresselhaus spin-orbit parameter, it depends on the thickness and effective width of the quantum wire and it can be varied with a split the potential of the gate, which controls the frequency of the oscillator and thus the effective width[19].

1.5 Zeeman Effect

Zeeman effect happened when an external magnetic field B applied in the materials then a sharp spectral lines splits into multiple lines.

Zeeman effect happened due to the interaction between the external magnetic field and the magnetic dipole moment. The magnetic dipole moment generated due to the motion of the electron charge and the spin motion of the electron itself.

an external magnetic field will exert a torque on a magnetic dipole and the magnetic potential energy which results in

$$U = -\mu\,.\,B$$

The magnetic dipole moment associated with the orbital angular momentum is given by

$$\mu_{orbital} = \frac{-e}{2m_e}\,L$$

Where is

$\mu_{orbital}$: the magnetic dipole moment.

e : the charge of electron.

m_e : the electron mass.

L: the orbital angular momentum.

For a magnetic field in the z-direction this gives

$$U = \frac{e}{2m} L_Z B = m_l \frac{e\hbar}{2m} B$$

Where is

B: the magnetic field

$\hbar$: Planck constant.

L_Z: the orbital angular momentum in Z direction.

When the quantization of angler momentum taken to account, the spaced energy levels given by:

$$\Delta E = m_l \frac{e\hbar}{2m} B$$
$$= m_l \mu_B B$$

Where is

ΔE: the average energy

μ_B : the Bohr magneton.

$$\mu_B = \frac{e\,\hbar}{2\,m_e} = 9.2740154 \times 10^{-24} \frac{J}{T} = 5.788382 \times \frac{10^{-5} eV}{T}$$

The Zeeman effect is the displacement of the energy levels gives uniform multiple splitting space of the spectral lines.

The magnetic dipole moment is the measurement of an object's propensity to line up with a magnetic field is known as a magnetic moment, sometimes known as a magnetic dipole moment. The magnetic pull and direction of a magnet or other item that generates a magnetic field are known as the "Magnetic Moment".

A vector quantity is the magnetic moment. The magnetic moment vector frequently aligns with the magnetic field lines when the objects are positioned in that way.

The magnetic moment of a magnet points from its south pole to its north pole. A magnet's magnetic moment is inversely proportional to the magnetic field it produces.

The magnetic moment is generated by the following two methods:

- The motion of Electric Charge.
- Spin Angular Momentum.

A magnetic dipole is made up of two opposing poles that are equally strong and spaced close together. For instance: Magnetic dipoles include objects like a bar magnet and a compass needle. We'll demonstrate how a current loop behaves like a magnetic dipole. Electrical Dipole The distance between the two poles multiplied by the pole strength is referred to as the moment. The magnet length, or 2l, is the distance between a magnet's two poles or a magnetic dipole. The magnetic dipole moment of the magnet is denoted by the vector M and is shown as if m is the power of any magnetic pole.

$$\overrightarrow{\mathrm{M}} = \frac{m}{2I}$$

The direction of the magnetic dipole moment, which is a vector, is from the magnet's south pole to its north pole.

1.6 Transverse Confinement Potential

Potentials that confine electrons in quantum dots (QDs) can possess various shapes depending on their origin and a structure of the QD**.** The confining potential stems from the band offsets and can be modified by the alloying and strain effects**.**

In the gated (electrostatic) QDs, the confinement potential is created by the external voltage applied to the gate and by the quantum well/quantum barrier structure. The confinement potential can be either obtained from the first-principles calculations assumed in some parametrized form, which allows us to model its shape.

When using the first method, it also appears to be helpful to find some parametrized analytic form of the confinement potential, which is useful in further applications. The

confinement potential is usually modelled by the two simple forms. It can be either the rectangular potential well or the parabolic (harmonic oscillator) potential.

It results from the numerical solution of the Poisson equation for the electrostatic QDs that the lateral confinement potential is nearly parabolic at the center of the QD and becomes non-parabolic at the QD boundary. The parabolic shape of the confining potential is consistent with the generalized Kohn theorem, which is approximately fulfilled in the far-infrared spectroscopy data. However, the parabolic potential possesses the infinite depth and range; therefore, it fails when trying to describe the charging of the QDs by the finite number of electrons. Recently, the Gaussian potential well with the finite depth and range has been introduced as a more realistic model confining potential in QDs.

Having at disposal an analytic, suitably parametrized, model confinement potential appears to be useful in calculations of the many-electron states in QDs. The confinement potential, that is both realistic and general enough to be applicable to a large class of the QDs, should possess the following properties:

(i) the finite depth and range, which result from the finite band offset and the finite size of the QD.

(ii) the anisotropy, since a large class of the QDs is anisotropic and usually possesses the approximate cylindrical symmetry.

(iii) the variable softness, which allows us to account for a compositional modulation and strain effects in the QDs.

(iv) the approximate parabolicity near the QD center.

The transverse confinement potential classified in the following equation:

$$V\ (\rho, z) = \ -V_o\ e^{\left[-\left(\frac{\varrho}{R}\right)p-\left(\frac{|z|}{Z}\right)p\right]}$$

Where is V_0 is the depth of the potential well (V_0>0). ϱ and z are the cylindrical coordinates, and $p\geqslant 1$. Since, in general, the QD possesses a different extension in the lateral (x,y) and vertical (z) direction, i.e., is anisotropic, we take this anisotropy into account by introducing the different ranges.

1.7 Nanowires Practical Applications

Due to their high extinction coefficient and rapid optical nonlinearities, quantum dots hold special promise for optical applications and could be used to create all-optical systems. They exhibit the Coulomb blockade phenomenon and work similarly to single-electron transistors. Quantum dots have also been proposed as active components for thermoelectric and as qubit implementations for quantum information processing. Numerous potential applications make tuning quantum dot size appealing. For instance, larger quantum dots exhibit less obvious quantum features and have a stronger spectrum-shift toward red than smaller ones. On the other hand, one can benefit from more subtle quantum effects by using smaller particles.

Quantum dots, which are zero-dimensional, have a sharper density of states than structures with greater dimensions. They consequently possess better optical and transport qualities. They could be used in biological sensors, amplifiers, and diode lasers. The surface plasmon resonance in the photoluminescent excitation spectrum of (CdSe)ZnS nanocrystals can be used to study how quantum dots are excited in a locally enhanced electromagnetic field created by gold nanoparticles. Optical encoding and multiplexing applications are well suited for high-quality quantum dots because of their broad excitation profiles and narrow/symmetric emission spectra. The study of intracellular processes at the single-molecule level, high-resolution cellular imaging, long-term in vivo cell trafficking observation, tumor targeting, and diagnostics are just a few of the many applications for the new generations of quantum dots. Triplet photosensitizers made of CdSe nanocrystals work effectively. The ability to extract the excited state energy from Quantum Dots into bulk solution through laser excitation of tiny CdSe nanoparticles opens the door to a wide range of possible applications, including photodynamic treatment, photovoltaic technology, molecular electronics, and catalysis.

Many devices use charges to encrypt the information like transistors. In their way to enhance the charged based devices, researchers considered the spin of electrons instead of charge to achieve low power devices with more functions. Spin-based devices or Spintronics promises to establish beyond-CMOS computing technology and to be applied in non-volatile magnetic random-access memory (MRAM), rotational speed control systems, programable logic devices, control devices in robotics. There is another class of spintronics devices called spin filed effect transistor (Spin-FET) which is considered to be

more suited for some applications like single-stage frequency multiplier due to its oscillatory transfer characteristics even it is not energy efficient comparing with MOSFET[20].

In quantum computing, Frolov et el. assessed in their research the use of semiconductor nanowires as platform material and it is power over conventional martials to enable more sophisticated operations, such as control over single degrees of freedom and their quantum states, in addition to preservation and coherent transferring of these states between distant nodes. And they as well reviewed recent experiments about using small bandgap nanowires in manipulating single spins in quantum dots and on Majorana fermions which are quasiparticles relevant for topological quantum computing[21] [22].

Designing complementary logic with spin-FETs Two complimentary spin-FETs that are comparable to the n- and p-type of traditional charge-based transistors are modelled. Parallel and anti-parallel spin-FETs are names for the complementary spin-based transistors. The orientation of the source and drain electrodes' magnetic fields in these two transistors is different. It is known as a parallel spin-FET if the magnetizations are mutually parallel, and it is known as an anti-parallel spin-FET if they are mutually anti-parallel. Only one transistor is conducting when these spin-FETs are utilized in a circuit with their gates shorted. The work's simulations are carried out using parameters based on a variety of experimental and theoretical findings. Since there are two different types of transistors in standard MOSFET-based logic designs. One is a p-type MOS and the other is an n-type MOS (PMOS). For any logic implementation in a traditional CMOS logic design, these two transistors are required.

A p-type substrate and n-type source and drain electrodes make up a PMOS transistor, whereas an NMOS transistor is made up of a p-type substrate and n-type source and drain electrodes. Because NMOS and PMOS transistors operate in complementary mode, this type of transistor is known as a complementary transistor. When the gate voltage is in the high state, the NMOS device is ON, whereas the PMOS device is ON when the gate voltage is in the low state. The fundamental concept behind this design is the substitution of parallel and anti-parallel spin-FETs for NMOS and PMOS (P Spin-FET and AP Spin-FET).

Fast moving electrons move while being affected by an electric field, which causes an effective magnetic field to be created by the Rashba effect [34]. As a result, the gate voltage applied from outside regulates the Rashba field, which in turn controls the current flowing through the channel.

Numerous initiatives have been made in order to propose and realize various material-based power-efficient, high-speed, and scalable spin-FETs with the development of spin-FET topologies. Additionally, a number of complementary spin-FET models and multi-gate spin-FET models have been proposed and simulated for use in the implementation of a number of digital logic circuits, such as NAND, XOR, NOT gates, and some higher-order functions like complete adders. The advancement made in this area shows that lessening the device and circuit footprint may be possible using this technology. The performance and manufacture of these devices continue to present significant problems, although recent advancements may have a significant impact on the creation of non-conventional CMOS electronics.

Following are a few spintronics applications:

- Mass-storage devices make use of spintronic technology. It is used to fit a lot of data into a tiny space; for example, a single-sided 3.5-inch disc can fit about 1 TB of data at 1.5 Gbit/mm2 or one trillion bits per square inch.
- The detection of cancer is another application of spintronics in medicine.
- The general field of spintronic technology has promise for digital electronics. It has been put to the test in mass-storage devices, specifically hard drives.

Future Spintronics Projects

- Optical or magnetic injection to produce spin polarization
- Spin-polarized interfaces between semiconductors and superconductors for transport
- Spin relaxation in semiconductors and metals
- Amplifiers and PN junctions are examples of spin-based electronics.
- Electron entanglement and spin-based quantum computation in many semiconductor devices[22]

1.8 Literature Survey

Spin-Orbit interaction (SOI) in semiconductors has received a huge attention from in recent years due to their wide application in future spintronic devices [23] [24] [25]. Electron's spin degree of freedom and charges are used for developing new spintronic device concepts. These new concepts aim at increasing speed and minimizing power consumption and to offer new functionalities that are not available in the existing electronic devices[19]. Rashba and Dresselhaus couplings are two basic mechanisms that affect SOI and spintronic devices structural as well [19], [26] [27]

In past two decades, many researches have studied the SOI of two-dimensional electron gases and have showed that studying one-dimensional channel is more suitable for improving the performance of spin transistor. Therefore, various research groups have investigated the spintronics in one-dimensional quantum wires with SOI. Moroz and Barnes (2003) shown the effect of Rashba SOI on the transport in one-dimensional systems at zero magnetic field.

Malet et al. (2006) have considered the effect of Rashba, Zeeman and Dresselhaus interactions on Landau levels in the quantum wells[28].

Zhang et al, (2009) studied the SOIs that resulted from Rashba, Dresselhaus and the lateral parabolic confining potential on the energy dispersion relation of the spin subbands in a parabolic quantum wire. In addition, they studied the effect of Zeeman that led to complex electro -subband for different spin branches.

K. Y. Bliokh, F. J. Rodríguez-Fortuño, F. Nori & A. V. Zayats (2015) described the primary spin-orbit interaction phenomena in optics, including their underlying causes and significant applications. These include spin-Hall effects at optical interfaces and in inhomogeneous media, spin-dependent effects in nonparaxial (focused or scattered) fields, spin-controlled light shaping using anisotropic structured interfaces (meta surfaces), and strong spin-directional coupling via evanescent near fields. We demonstrate that spin-orbit interactions are fundamental to all fundamental optical processes and are essential to contemporary optics[29].

Tin-Lun Ho and Shizhong Zhang (2011) investigated a broad method for producing gauge field families in the scalar, spin-orbit, and non-Abelian regimes. All of these can

theoretically be accomplished by the NIST experiments, which modify the spin state of bosons while imparting momentum to them. They demonstrate that a Bose gas is a spinor condensate composed of two non-orthogonal dressed spin states carrying various momenta in the spin-orbit regime. As a result, its density exhibits a striped pattern with contrast proportional to the overlap of the dressed states. By changing the experimental settings, this pattern can be made to appear highly strong[30].

G.Bihlmayer , Yu.M.Koroteev ,P.M.Echenique, E.V.Chulkov and S.Blügel (2006) Used contrasting structure - based calculations for Au(1 1), Ag(1 1), and Lu(0 0 0 1), they examine the prerequisites for such a Rashba-effect at metallic surfaces and look into the effects of electric and magnetic (exchange) forces on these surface states[31].

Rajab, Hanaa Sameer (2021) studded the findings show that the Rashba effect, temperature, and confining frequency have a significant impact on the magnetic properties of the QD, converting it from a diamagnetic to a paramagnetic state in the InAs material, while GaAs maintains its diamagnetic state at a range of magnetic field strengths. The behavior of the heat capacity and entropy is examined in relation to the quantum dot parameters and the external magnetic field. The findings show that the Rashba effect, temperature, and confining frequency have a significant impact on the magnetic properties of the QD, converting it from a diamagnetic to a paramagnetic state in the InAs material, while GaAs maintains its diamagnetic state at a range of magnetic field strengths. The behavior of the heat capacity and entropy is examined in relation to the quantum dot parameters and the external magnetic field. There findings are quantitatively in excellent agreement with those found in the literature[32] .

Doina BEJAN1, Cristina STAN2, and Alina PETRESCU-NIȚĂ (2022) proposed a theoretical investigation into the effects of the Zeeman effect, the Rashba and Dresselhaus spin-orbit couplings, and the position of the donor impurity on the magnetic characteristics of a GaAs/GaAlAs pseudo-elliptic quantum ring. They discovered that the impurity's effects on magnetization are strongest when it is positioned in the middle of the ring. Using both Boltzmann and Fermi-Dirac statistics, the average total energy, the magnetization, and the magnetic susceptibility were calculated. Both distributions result in linear fluctuations of the magnetization vs the magnetic field if the electron spin is not taken into account. The ring is diamagnetic and exhibits a small increase in susceptibility with

magnetic field. When electron spin is taken into account, the susceptibility for the Fermi-Dirac distribution drops slowly with the field but displays a bigger Boltzmann distribution, if employed, will decrease with the magnetic field. In the latter instance, the middle-located impurity ring is paramagnetic in weak magnetic fields and diamagnetic in stronger magnetic fields[33].

Wan-Tsang Wang, C. L. Wu, S. F. Tsay, M. H. Gau, Ikai Lo, H. F. Kao, D. J. Jang, *and* Jih-Chen Chiang (2007) used the nearest-neighbor tight-binding approach, the spin-splitting energies of the conduction band for perfect wurtzite materials are computed. It is discovered that the ideal wurtzite bulk inversion asymmetry provides a minimum-spin-splitting surface, which can be thought of as a spin-degenerate surface in the form of $bk2z-k2\|=0$ ($b\approx4$) close to the point, in addition to a spin-degenerate line (along the kz axis). In bulk wurtzite materials, this phenomenon is known as the Dresselhaus effect (also known as the cubic-in-k term) because it causes a term known as γwz $(bk2z-k2\|)(\sigma xky-\sigma ykx)$ to appear in the two-band $\boldsymbol{k}\cdot\boldsymbol{p}$ Hamiltonian. The National Research Council of Taiwan and Academia Sinical provided funding for this project[[34]

M El-Said (1994) studded For various wire widths, the absorption coefficient of the donor impurity in the center of a quasi-1D GaAs quantum well wire is estimated as a function of photon energy. Investigated is the effect of a uniform magnetic field applied along the wire's axis on the optical spectrum connected to the bound-to-band transition of electrons from the donor ground state to the first conduction subband[35].

By employing a combination of variational and precise diagonalization techniques to solve the relative Hamiltonian, M.K. Elsaid∗ and E. Hijaz (2017) can determine the magnetic susceptibility of two interacting electrons that are contained in a linked double quantum dot and placed in a magnetic field. they have looked into how temperature, magnetic field strength, confinement frequency, and barrier height affect magnetic susceptibility. The magnetic susceptibility curve jumps that correlate to the singlet-triplet transitions in the quantum dot spectra's ground state have been demonstrated[36]

Mohammad K. Elsaid, Amal Abu Alia, Ayham Shaer (2020) have been examined the magnetic and thermal characteristics of a parabolic GaAs quantum dot based on the effective mass approximation in the presence of donor impurity, Rashba Spin-Orbit

interaction (RSOI), and applied magnetics and electric fields. The Hamiltonian of an electron contained in a quantum dot (QD) has been solved using the precise diagonalization approach in order to determine the eigenenergy's and the binding energy of the donor impurity as functions of different QD physical characteristics. they have demonstrated the relationship between the Rashba interaction parameter, the magnetic and electric fields, confinement frequency, and temperature and the average statistical energy, magnetization, magnetic susceptibility, and heat capacity of the donor impurity in the QD [37]

The magnetic and thermal characteristics of a parabolic GaAs quantum dot have been examined by Ayham SHAER, Mohammad K. ELSAID and Musa ELHASAN (2016) based on the effective mass approximation in the presence of donor impurity, Rashba Spin-Orbit interaction (RSOI), and applied magnetic and electric fields. The Hamiltonian of an electron contained in a quantum dot (QD) has been solved using the precise diagonalization approach in order to determine the eigenenergies and the binding energy of the donor impurity as functions of different QD physical characteristics. They have demonstrated the relationship between the Rashba interaction parameter, the magnetic and electric fields, confinement frequency, and temperature and the average statistical energy, magnetization, magnetic susceptibility, and heat capacity of the donor impurity in the QD [38].

By utilizing both variational and exact diagonalization techniques to solve the relative Hamiltonian, it was possible to determine the magnetization of two interacting electrons that were contained in a linked double quantum dot and displayed in a magnetic field. Hjaz, Eshtiaq; Elsaid, Mohammad K.; Elhasan, Musa (2017) have looked into the relationship between temperature, magnetic field intensity, confining frequency, and barrier height and magnetization. The magnetization curve jumps that correlate to the singlet-triplet transitions in the quantum dot spectra's ground state have been demonstrated [39]

At a fixed temperature and under the effect of external slanted electric and magnetic fields, Amal Abu Alia, Mohammad K. Elsaid, Ayham Shaer have

been explored how the magnetization and magnetic susceptibility of the donor impurity in the parabolic GaAs quantum dot relate. The Hamiltonian of an electron contained in a parabolic quantum dot with a donor impurity that is present in electric and magnetic fields has been solved using the numerical diagonalization approach of the Hamiltonian matrix, which is based on the effective mass approximation. The analytical forms of all the energy matrix components have been obtained. They have demonstrated how the strength of the electric and magnetic fields as well as the tilt of the electric field affect the statistical energy and binding energy of donor impurities [40]

Sajal Dhara, Hari S. Solanki, Vibhor Singh, Arjun Narayanan, Prajakta Chaudhari, Mahesh Gokhale, Arnab Bhattacharya, and Mandar M. Deshmukh examined each InAs nanowire's magneto transport characteristics in a field-effect transistor architecture. They observed magnetoresistance in the low magnetic field region, which is well captured by the weak localization description in diffusive conductors. As the gate voltage is raised, the weak localization correction becomes weak antilocalization. they demonstrated that the spin-orbit length and phase coherence length may be tuned by a factor of 2 using the gate voltage. They are noticed that the mobility of devices can be dramatically changed as a function of magnetic field in the high field and low temperature domain. they contend that in order to comprehend high-field magneto transport in nanowires, it is crucial to understand the function of skipping orbits and the characteristics of surface scattering [41]

The oscillations in universal conductance that are measured by Ch. Blömers, M. I. Lepsa, M. Luysberg, D. Grützmacher, H. Lüth, and Th. Schäpers (2011) under a perpendicular magnetic field provide information on the electron phase coherence. The phase-coherence length could be quantified by examining the universal conductance variations pattern of a number of nanowires of various lengths. Indicators of a strong flux cancelation effect were also discovered, and this is attributable to the nanowire's structure. they also provide measurements using a parallel arrangement of the wire and magnetic field. they do not observe periodic oscillations of the magnetoconductance in this structure, which is in contrast to earlier findings on InN and InAs nanowires. There is a proposed explanation for this pattern based on the high density in this setup, we do not see periodic oscillations of the magnetoconductance. It is proposed that the high density of stacking faults in our InAs wires explains this phenomenon [42]

By using a unique shadow evaporation technique for the superconductor electrode, Pujitha Perla , H. Aruni Fonseka , Patrick Zellekens , Russell Deacon , Yisong Han, Jonas Kölzer , Timm Mörstedt , Benjamin Bennemann , Abbas Espiari, Koji Ishibashi, Detlev Grützmacher, Ana M. Sanchez , Mihail Ion Lepsa and Thomas Schäper (2021) based on InAs semiconducting nanowires and Nb superconducting electrodes are created in-situ. Nb has the benefit of having a greater superconducting gap than other metallic superconductors like Al, which enables functioning at higher temperatures and magnetic fields. By growing pairs of InAs nanowires preferentially on two neighboring tilted Si (111) facets and crossing them at a minimal distance, we are able to create our junctions. The spacing between the superconducting electrodes on the lower nanowire is determined by the position of the top wire with respect to the deposition source using a shadow mask. Measurements using electron microscopy demonstrate that a clear InAs/Nb contact is produced by the entirely in situ production process[431.

Faten BZOUR , Mohammad K. ELSAID & Ayham SHAER (2017) proposed a theoretical investigation of the two-electron GaAs parabolic (Magnetic)'s susceptibility under the combined influence of external pressure, temperature, and magnetic field. By solving the two electron quantum dot Hamiltonian while taking into consideration the dependence of the effective mass and dielectric constant on the hydrostatic pressure and temperature, they employed the precise diagonalization method to derive the eigenenergy's. The computed QD spectra are significantly impacted by pressure and temperature. The behavior of a quantum dot's magnetization in relation to external pressure, temperature, confinement frequency, and magnetic field is then examined. The magnetic susceptibility spectrum's associated leaps and the singlet-triplet transitions in the ground state of quantum dot spectra have been demonstrated [44].

Elsaid et al, (2019) studied the magnetic properties of GaAs parabolic quantum dot [45] [46] [47] [48].

In this work, we have studied effects of full SOI like Rashba and lateral confinement term on the energy spectra and magnetic properties of the InAs quantum wire. The dependence of magnetization and susceptibility on the Rashba and Dresselhaus strength parameters, the magnetic field strength and the temperature, our results are explicitly presented in chapter 3.

1.9 Research Objectives

Main goals of this thesis are:

1. We have solved the Hamiltonian problem of a single electron confined in a InAs QWW in the presence of Rashba, Dresselhaus, lateral SOI, Zeeman effect and applied uniform magnetic field by using exact numerical diagonalization technique, and computed the eigenenergies and eigenfunctions.
2. We have solved the effect of temperature on the average energy at certain values of Rashba parameter firstly, then with Rashba and Dresselhaus parameters and external magnetic field.
3. The obtained eigenenergies have been used to investigate the behavior of the magnetic properties of the InAs QWW by calculating the Magnetization (M), magnetic Susceptibility (χ) of InAs QWW nanomaterials at temperature range (0.1, 10 K).

Chapter Two

Theory and Method of Calculations

This chapter shows the Hamiltonian of an electron confined in QWW by an external electric and magnetic fields with Rashba and Dresselhaus SOI. After calculating all the energy matrix elements terms in QWW Hamiltonian model, we solved the Schrodinger equation by using exact numerical diagonalization techniques to obtain the eigen energies and eigenfunctions of the one-dimensional nanosystem($\langle\psi_n|\hat{H}|\psi_m\rangle, |\hat{H}nm - EI| = 0$) the basis function ψ_n are taken to be well-known Harmonic oscillator or Hermite basis, $\hat{H}_n(x)$. The obtained eigen energies were used as input parameters to compute the partition function from which used to calculate the magnetic properties of the QWW, the Magnetization and Susceptibility.

2.1 QWW Hamiltonian

The Hamiltonian of an electron confined in a QWW in the presence of an electric and magnetic field can be written as:

$$\hat{H} = \frac{1}{2\,m^*}\,(\,\hat{p} + e\,A\,)^2 + \frac{1}{2}\,m^*\,\omega_0^2\,x^2 + \frac{1}{2}\,g^*\,\mu_B\,\overrightarrow{B}\sigma_z + \alpha_R\,\frac{1}{\hbar}\,[\,\sigma\,\times(\,\widehat{p} + e\,A\,)]_z + \beta_D\,\frac{1}{\hbar}\,[\,\sigma_y\,(\,\widehat{p_y} + e\,B_x\,) - \sigma_x\,\widehat{p_x}\,] + \frac{\gamma}{\hbar}\frac{X}{l_0}\sigma_z(\widehat{p_y} + eB_X) \qquad (2.1)$$

1. The first term of the Hamiltonian is the kinetic energy, where the quantity($\hat{\mathrm{p}} + \mathrm{e}\,\vec{\mathrm{A}}$) known as canonical (total) momentum ; $\hat{p}$ is the momentum operator, $\boldsymbol{e}\,\vec{\boldsymbol{A}}$ is the potential momentum (momentum in field) due to interaction with constant magnetic field acting on the Z-direction on the QWW, in which potential energy depend explicitly on velocity, $m*$ is the effective mass of the electron ($m^* = \frac{1}{\hbar^2}\,\frac{\partial^2 E}{\partial\,k^2}$)[33], e is the electron charge and $\boldsymbol{A}$ is a magnetic vector potential in the Lande gauge $\boldsymbol{A} = (0, Bx, 0)$.
2. The second term is a confinement parabolic potential representing the restriction of the motion of charge carrier, where ω_0 is the frequency of confinement potential.
3. The third term is Zeeman energy splitting with g^* the effective Lande factor, μ_B is the Bohr magneton where:

$$\mu_B = \frac{e\,\hbar}{2\,m_0 c} \tag{2.2}$$

, $\boldsymbol{\sigma}$ are Pauli spin matrices and $\vec{B}$ representing the magnetic field vector in Z-direction, i mean the magnetic field perpendicular to the InAs-QWW material.

4. The fourth term is the Rashba SOI arises from the asymmetry of the qumtum well induced by a uniform interface induced field or by external applied gate voltage along z-axis (the interaction between orbital angular and spin momenta), where α_R is the Rashba spin-orbit coupling parameter, which can be varied by the gate electric field.
5. The fifth term represents the Dresselhaus SOI Hamiltonian, where β_D is the Dresselhaus spin-orbit coupling parameter.
6. The last tern represents the Hamiltonian of SOI coming from transverse confining potential. Where $\widehat{H}_{SO}^{T}$ is:

$$\widehat{H}_{SO}^{T} = \frac{\gamma}{\hbar}\frac{x}{l_0}\,e_x\left[\vec{\sigma}\times\left(\vec{p}+e\,\vec{A}\right)\right] \tag{2.3}$$

Where γ is the spin-orbit coupling parameter. l_0 is the length scale which characterize the strength of lateral confining potential.

$$l_0 = \sqrt{\hbar/m^*\omega_0} \tag{2.4}$$

2.2 Magnetization

Magnetization (M) is a property of the QWW, which explain how the material responds to the external magnetic field. We can calculate the magnetization by[49]:

$$M = -\frac{\partial <E\,(\omega_c,\alpha_R,\omega_0,T,S)>}{\partial B} \tag{2.5}$$

Where $< E(\omega_c, \alpha_R, \omega_0, T, S) >$ is average energy,

$$< E_n\,(\omega_c, \alpha_R, \omega_0,, T, S) > = \frac{\sum_{n=1}^{N} E_n e^{-\frac{E_n}{K_B T}}}{\sum_{n=1}^{N} e^{-\frac{E_n}{K_B T}}}. \tag{2.6}$$

The density of induced or permanent dipole moments in a certain magnetic material is measured by magnetization, also known as magnetic polarization. We already know that the magnetic moment, which is produced by the mobility of electrons within atoms, the

spin of electrons, or the nuclei, results in magnetization. In addition to any unbalanced magnetic dipole moment that is present due to the motion of the material's electrons, as was previously discussed, the response of a material to the external magnetic field determines its net magnetization. We can categorize materials according to their magnetic properties with the aid of the idea of magnetization.

The net magnetic moment for a given sample material M can be thought of as the magnetization of that substance per unit volume. Mathematically,

$$M = \frac{m_{net}}{V}$$

Now let's look at the situation of a solenoid. Take a solenoid with n turns per unit length and let I represent the current flowing through it. From this, the magnetic field inside the solenoid can be calculated as follows

$$B_\circ = \mu_\circ n\, l$$

The field within the solenoid must now be stronger than previously if we fill the interior with a material having a non-zero magnetization. The solenoid's internal net magnetic field B can be expressed as

$$B = B_\circ + B_m$$

Where B_m gives the field contributed by the core material. Here, B_m is proportional to the magnetization of the material, M. Mathematically,

$$B_m = \mu_\circ M$$

Here, μ_0 is the constant of permeability of a vacuum.

Let us now discuss another concept here: a material’s magnetic intensity. The magnetic intensity of a material can be given as

$$H = \frac{B}{\mu_\circ} - M$$

Here, the magnetic field due to the core's nature is denoted by M, and the magnetic field due to external causes like the solenoid's current is denoted by H. The latter quantity, M, is determined by outside factors and is given by

$$\mu = \chi H$$

where is the χ magnetic susceptibility. It gauges how a substance reacts to an outside force. For paramagnetic and diamagnetic materials, respectively, the magnetic susceptibility of a material is small, positive, and small, negative.

$$\begin{aligned} B &= \mu_\circ (1 + \chi) H \\ &= \mu_\circ \mu_r H \\ &= \mu H \end{aligned}$$

Here, the term μ_r is termed as the relative magnetic permeability of a material, which is analogous to the dielectric constants in the case of electrostatics. We define the magnetic permeability as[50]

$$\begin{aligned} \mu &= \mu_\circ \mu_r H \\ &= \mu_\circ (1 + \chi) \end{aligned}$$

2.3 Magnetic Susceptibility

Similarly, the magnetic Susceptibility (χ) explains how material changes due to applied external magnetic field, it classifies the material into diamagnetic when $(\chi < 0)$, paramagnetic when $(1 > \chi > 0)$ and ferromagnetic when $\chi > 1$ [51].

By taking the derivate of Magnetization with respect to the magnetic field B, we can calculate the magnetic Susceptibility, as:

$$\chi = \frac{\partial M}{\partial B} \tag{2.6}$$

A material's magnetic susceptibility reveals whether it is drawn into or repelled by a magnetic field. Materials that are paramagnetic align with the applied field and are drawn to areas with stronger magnetic fields. Diamagnetic materials are pushed away and anti-aligned in the direction of lower magnetic field areas. The magnetization of the material adds its own magnetic field on top of the applied field, which causes the field lines to concentrate in paramagnetic or be excluded in diamagnetism. Quantitative measurements of the magnetic susceptibility can shed light on bonding and energy levels inside a material's structure. Additionally, it is commonly utilized in geology for structural geology and paleomagnetic research.

The magnetic atomic-level characteristics of the constituent particles of materials determine their magnetic susceptibility. Typically, the magnetic moments of electrons control this. All materials contain electrons, but in the absence of an external magnetic field, the electrons' magnetic moments are often paired or random, leaving no overall magnetism (the exception to this usual case is ferromagnetism). The underlying causes of whether or not the magnetic moments of the electrons line up are extremely complicated and cannot be deduced from conventional physics. To simplify things, one can measure a material's magnetic susceptibility and utilize the macroscopic form of Maxwell's equations. Due to this, classical physics can make valuable predictions without being subject to the details of the underlying quantum mechanics[52].

Chapter Three

Results and Discussion

In this chapter we will present the numerical calculations for Rashba, Dresselhaus SOI and transverse confining potential on a single electron confined by a parabolic confinement potential in a QWW made from InAs-material. We further study the Magnetization and Magnetic Susceptibility of InAs- material.

The material parameters for InAs-QWW that we have used in our calculation are given in Table 3.1[53]

Table 3.1

Material parameters of InAs-QWW

Effective mass of the electron (m^*)	Effective Lande Factor (g^*)	Effective Rydberg (R^*)	Effective Bohr radius(α^*)	Cyclotron frequency (ω_c)
0.042 m_0	14	2.68 *meV*	18.39 *meV*.nm	0.97 *meV*

3.1 Energy Dispersions Relation

Firstly, we have tested the program code that we used to get out the standard QWW energy results.

En[B_(*in Tesla*),wo_(*in meV*),\[Alpha]_(*in nm.meV*),\[Beta]_(*in nm.meV*),ky_(*Number*),Ef_(*10KV/cm*),nmax_,dd_]:=RankedMin[Eigenvalues[Partition[Flatten[Table[matelemE[B,wo,\[Alpha],\[Beta],ky,Ef,n,nn,\[Sigma],\[Sigma]\[Sigma]],{n,0,nmax},{\[Sigma],-1,1,2},{nn,0,nmax},{\[Sigma]\[Sigma], 1,1,2}]],(nmax+1)*2]]*ref,dd](the mathematical code that we tested)

The obtained results of the dispersion energy for GaAs-material was compared with the corresponding ones results and the results matched.

calculated by Tong-Yi Zhang et el[19]. Figure 3.1 shows the energy dispersion for GaAs-material at different values of magnetic field (B), α_R and $\beta_{D.}$

Figure. 3.1

Energy Dispersion for GaAs of spin splitting

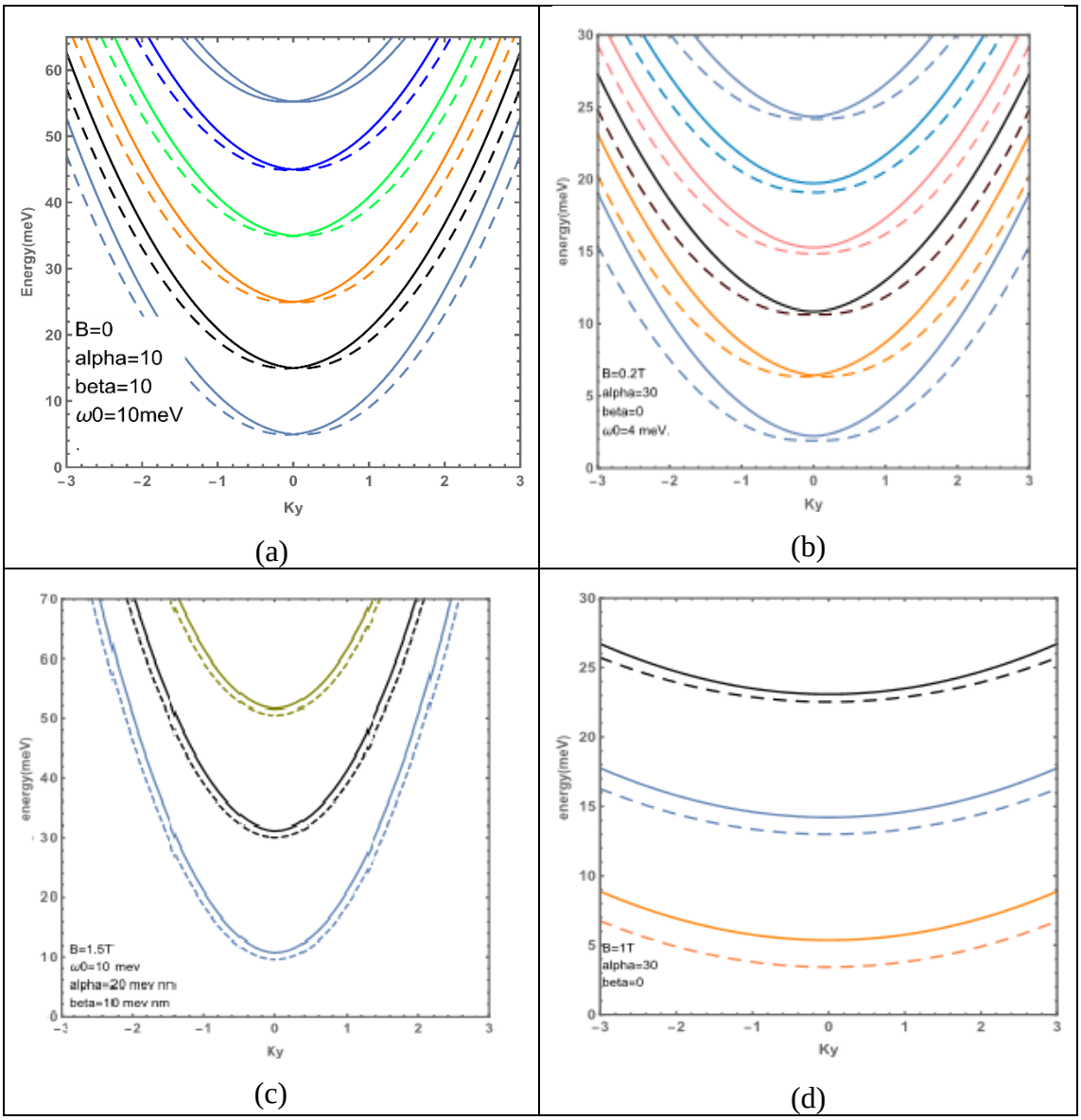

* (a) B=0T, α_R= 10 nm .meV, β_D= 10 nm meV, $_\gamma$ =0 nm meV, ω_0=10 meV. (b) B=0.2T, α_R= 30 nm .meV,β_D= 0 nm. meV, $_\gamma$ =0 nm .meV, ω_0=4 meV. (C) B=1.5T, α_R= 20 nm meV,β_D= 20 nm meV, $_\gamma$ =0 nm .meV, ω_0=10 meV. (d) B=1T, α_R= 30 nm .meV, β_D= 0 nm .meV, $_\gamma$ =0 nm meV, ω_0=4 meV.

After we have tested the code on GaAs, we used it to calculate the energy dispersion (Energy versus K_y) for InAs-material under Rashba, Dresselhaus and Zeman effects. We have three variables that effect on the dispersion of the energy states of material and these are: the magnetic field (B), Rashba term α_R and Dresselhaus term β_D.

Firstly, we fixed β_D = 0 nm meV and B=0T and we plot energy dispersion at different values of α_R to study the effect of Rashba effect on Energy states of the QWW.

Figure 3.2 shows the Energy versus the wave vector K_y at different values of α_R and fixed value of B=0T and Dresselhaus effect neglected ($\beta_D = 0$). From the graphs, the splitting of states increase when α_R increase and the degeneracy decreases.

Figure 3.2

Energy Dispersion splitting of InAs-material at B=0T and β_D=0nm $.meV$

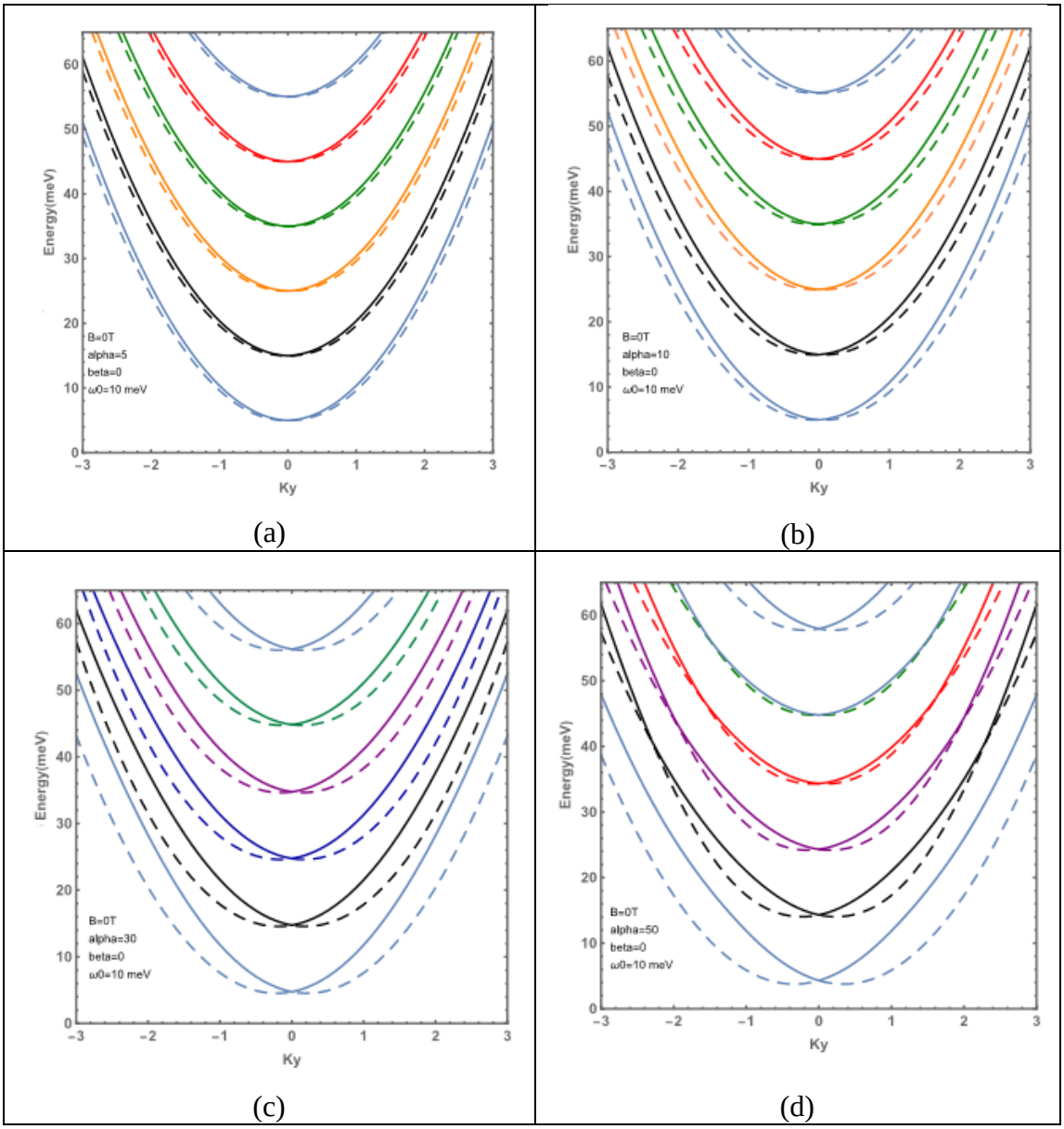

* (a) α_R = 5 nm .meV. (b) α_R = 10 nm .meV . (c) α_R = 30 nm . meV. (d) α_R = 50 nm .meV.

Next step, we add a magnetic field with Rashba and kept β_D=0. Figure 3.3 shows the Energy dispersion for InAs at different values of α_R with magnetic field. The splitting of states become larger than the splitting in the first case i.e., at B=0 T.

Figure 3.3

Energy Dispersion splitting of InAs-material at B=1T and β_D=0nm meV

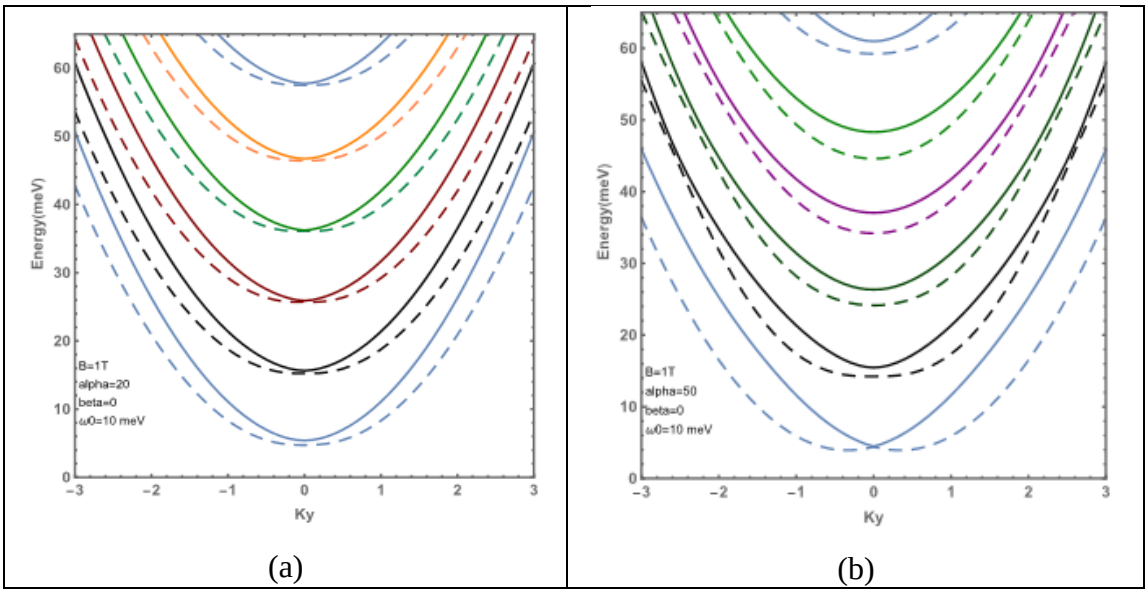

* (a) α_R = 20 nm. meV. (b) α_R = 50 nm .meV

In Figure 3.4 we take Rashba and Dresselhaus effects together i.e., β_D now has a finite value: β_D = 1/2 α_R. Here the energy dispersion becomes larger as shown in Figure 3.4. Firstly, we take B=0T.

Figure 3.4

Energy Dispersion splitting of InAs-material at B=0T

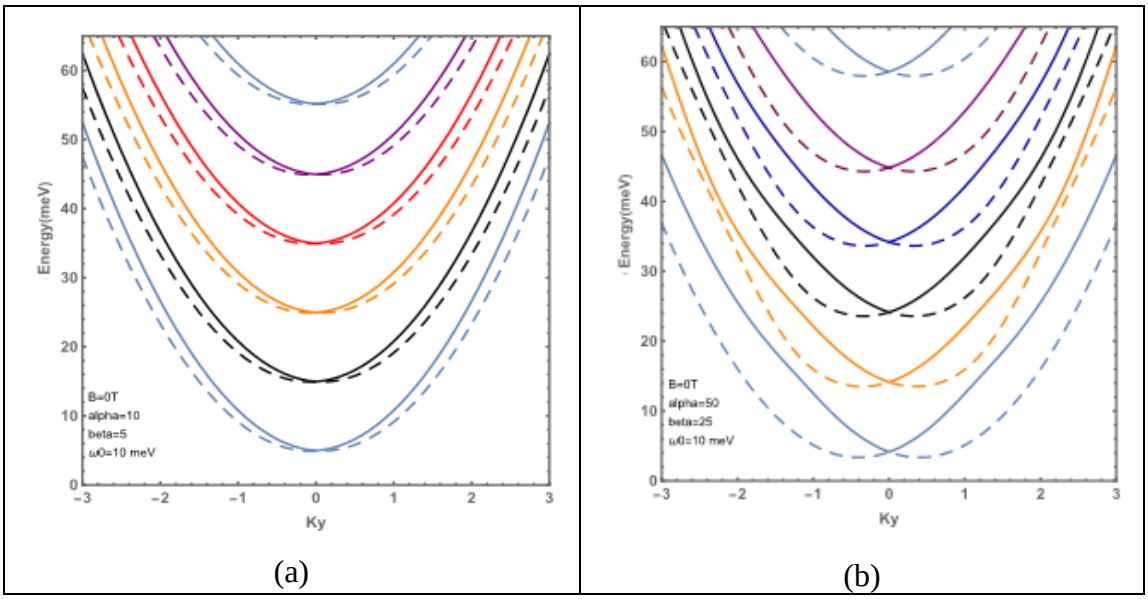

* (a) α_R = 10 mev,nm and β_D=5meV.nm (b) α_R = 50 meV.nm, and β_D=25meV.nm.

To investigate the effect of magnetic field, Rashba and Dresselhaus, energy dispersion have been done in Figure 3.5 for different values of $\alpha_{R,\,\beta D}$ at different values of B, and the splitting of energy states becomes clearly very large at high values of Rashba and Dresselhaus values and magnetic field. This mixed effects lifts the level degeneracy.

Figure 3.5

Energy Dispersion splitting of InAs-material

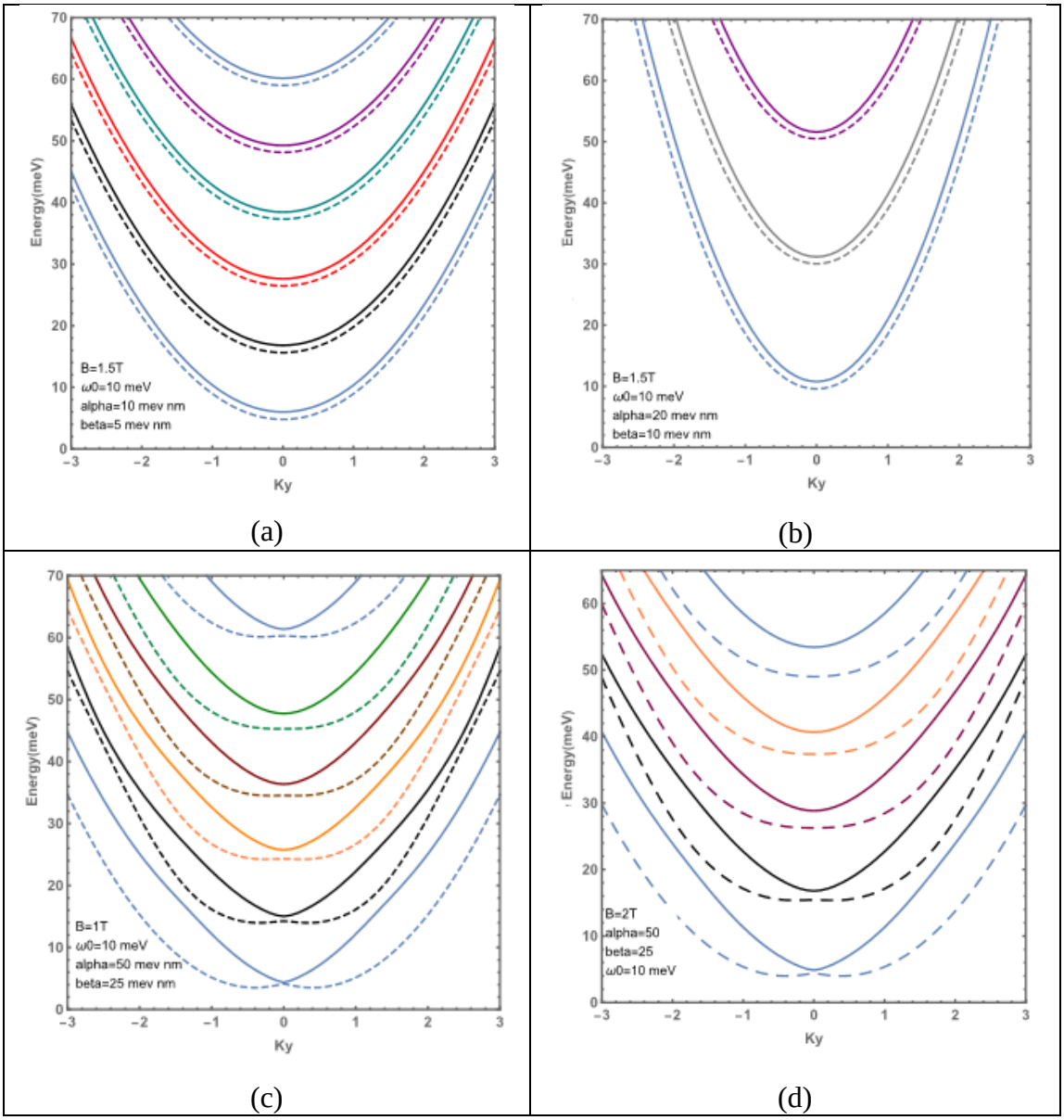

* (a) αR = 10 meV,nm βD=5 meV,nm B=1.5 T. (b) αR = 20 meV.nm, βD=10 meV.nm, B=1.5T.(c) αR = 50 nm. meV, βD=22 meV,nm B=1T.(d) αR = 50 meV.nm, βD=25 meV.nm, B=2T.

3.2 Average statistical Energy

In this section we will show the effect of Rashba and Dresselhaus terms on the average energy E_{avg} of InAs QWW material. We have diagonalize the QWW Hamiltonian given by Eq. (2.1), and compute the energy eigenvalues and the eigenfunctions of the sub bands of QWW numerically. In all the computational processes, we have checked the convergency of the average energy given by equation. For example, the average energy plot against state number of bases (states) (n) at T=0.1 K, $\alpha = 50\ meV$.nm and $\beta = 25\ meV$ .nm shown in Figure 3.6.

Figure 3.6

*Number of bases "n" Vs. Average energy (**meV**) at T=0.1K, α=50 **meV** nm and β= 25 **meV**. nm*

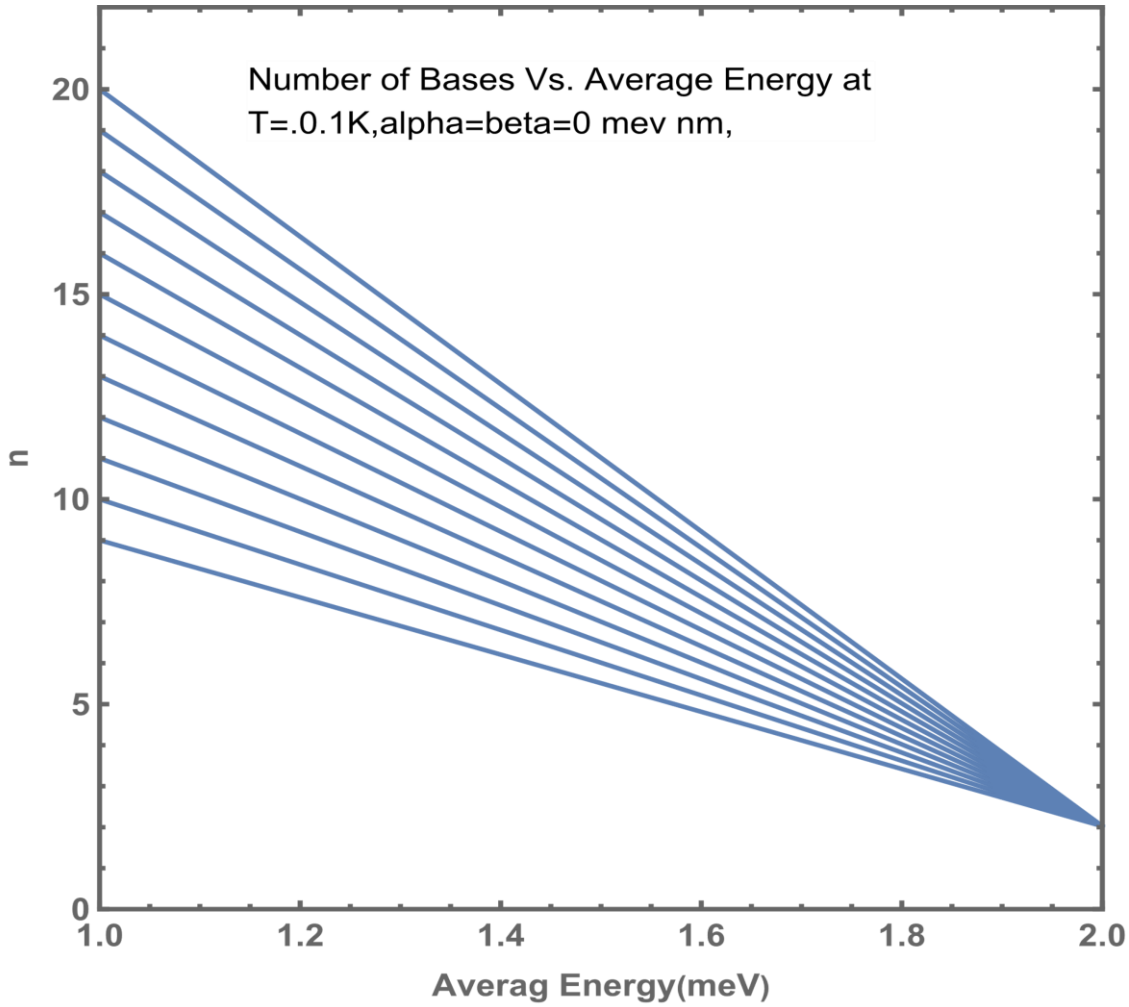

We have studied the temperature effects on average energy for two different cases, the First case, we take some values of α for fixed B= 1T, β =0 *meV*. nm to see the effect of

Rashba case alone. Figure 3.7.(a) clearly shows a plot of average energy as a function of T. However, that at certain value of α the average energy increases when T increase. As α increases the average energy as a function of T curve retracts downward.

Figure 3.7.a

The Average Energy (meV) versus T(K) at B=1T and β=0 meV.nm

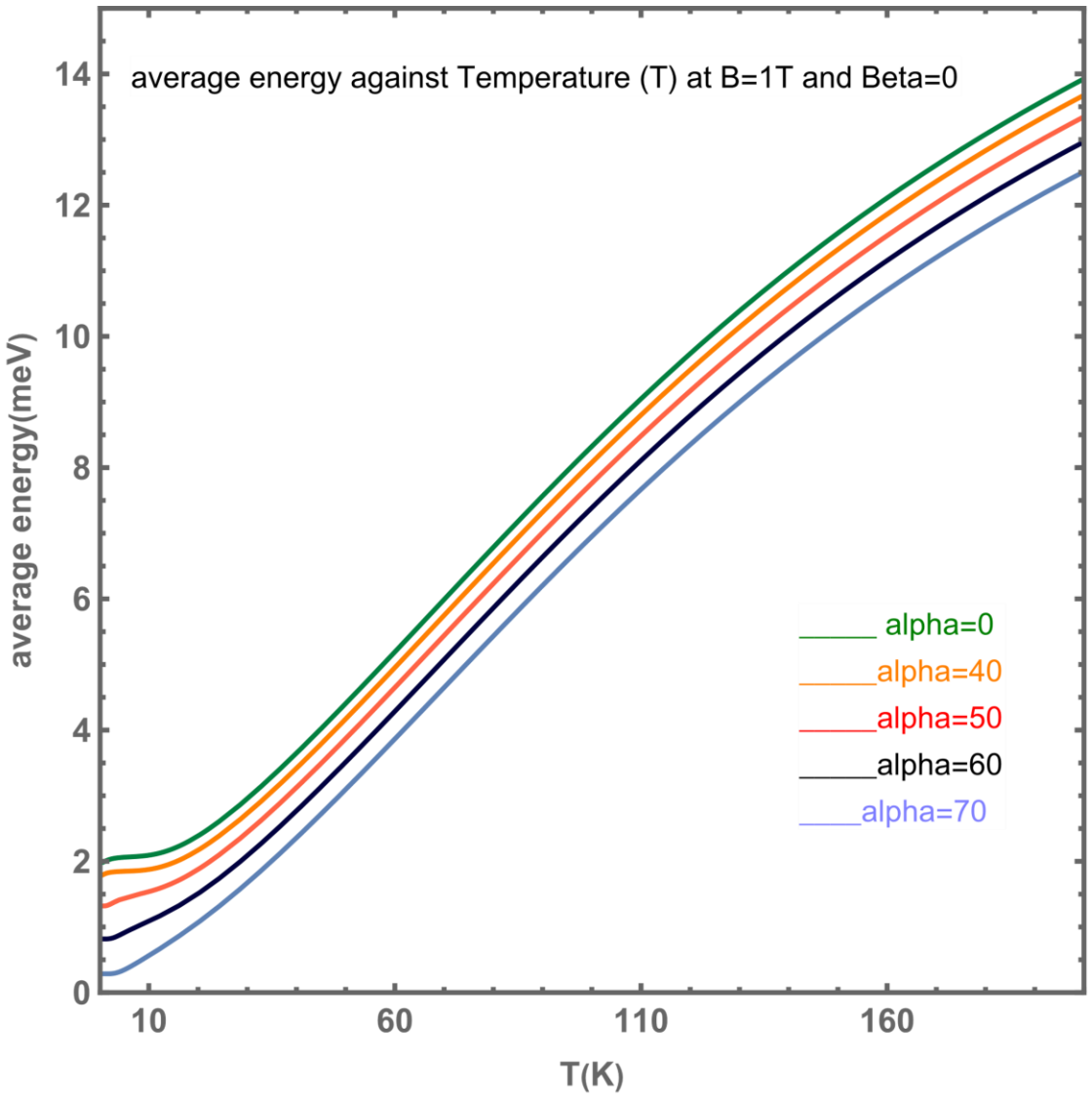

Secondly, we took in to account Dresselhaus and Rashba effects too. Figure 3.7.(b) -see Appendix A- shows the plot of Average energy as a function of T at B =1T and β=1\2 α, we can see that the curves shifts downwards and this shifting energy is larger than the first case i.e., at β_D=0 *meV*.nm. This shows the importance of having a Rashba and Dresselhaus effect simultaneously**.**

After that, we study the effect of magnetic field on average energy at particular value of temperature T i.e., the effect of increasing Zeeman term with Rashba alone, and with Rashba and Dresselhaus together, second, on the average energy of InAs QWW. At $\beta_D = 0\ meV.$ nm, we have taken low (0.1K) and high(10K) temperature values. Figure 3.8. a -see Appendix A- represents a plot of average energy as a function of B at T=0.1K and for different values of α_R. Note that at low B value, the Rashba term has more effect than at high B value, because of the energy competition between Rashba and B quantities and this competition makes the energy separation less than at low B value. Note that at high B and at $\alpha_R = 0{,}40\ and\ 50\ mev.nm$ the degeneracy clearly appeared but at $\alpha_R = 60 and\ 70\ mev.nm$ the degeneracy removed.

In Figure 3.8.b -see Appendix A- we have the plotted average energy against B at T=10K and $\beta_D = 0$ *meV*.nm. we have seen that the separation of energy states become larger due to the effect of T, the curves of average energy states shift up and Rashba effect becomes clear at low and high B limits.

In the plot, Figure 3.9.a and b -see Appendix A-, we have taken β=1\2 α at T limits (0.1& 10 K) and plotted average energy curves as a function of magnetic field.

At T=0.1K, we have seen that the effect of Rashba and Dresselhaus together is clear at low and high B, which that means the separation of the energy states becomes larger than in the first case i.e., at β_D =0 *meV.* nm. This shows again, the significant of including the Dresselhaus and Rashba effects together to remove the level degeneracy at high magnetic field. At T=10K, all average energy curves are shifted up,as expected, the energy becomes enhanced at higher T.

3.3 Magnetization and Susceptibility

In this section we present the computed results of magnetization (M) and susceptibility (χ) for InAs-QWW under the combined effects of Rashba and Dresselhaus SOI-terms and applied magnetic field.

Figure 3.10 -see Appendix A- represents a plot of M as a function of magnetic field B with four different numerical values of Rashba SOI parameter α_R (0,40,50,60 *meV.* nm), with β_D =0 *meV.* nm and low temperature (T=0.1K). The graph shwos that at α_R = 0 *meV.*

nm the magnetization curve does not show peak structure and it decreases as the magnetic field increases because of the effect of magnetic field in dipole moment, as we know magnetization is the the vector field that expresses the density of permanent or induced magnetic dipole moments in a magnetic material.

As we switch on the Rashba term, as α_R =40 *meV*. nm we have two peaks appear at B ~ 1.56 T and B~1.67 T and these peaks reflect the change in the magnetization from decreasing to increasing behaviors (diamagnetic to paramagnetic). This indicates a transition of a magnetic phase for InAs-QWW material. As α_R increases, the peaks shift towards a high magnetic field range. For α_R = 50 *meV*. nm the first peak occurs at B ~3.02 T then M increases up to reach the second peak at B ~3.12 T, and then M returns back to decrease again. At α_R= 60 *meV*. nm the peaks shift right again. The first peak occurs at B ~ 4.64 T then the magnetization increases up to B~4.7T and M returns to decrease again.

We fixed the Rashba parameters, and plot M against B at high temperature T=10K. At high T, all peaks in the $M-$ curves disappear for all the range of magnetic field from zero to 5T. That because of the shifting of the energy states upward. The exist thermal energy makes the dipole moment more random. Figure 3.11 -see Appendix A- shows the behavior of the Magnetization curve as a function of B at T=10K and four different values of α_R and for vanishing Dresselhaus effect β_D =0 *meV* .nm.

The plot in Figure 3.11 shows that all curves of M shift down at high T compered to 0.1K i.e., the magnetization of InAs-QWW material decreases when the temperature increases under Rashba and in the presence of magnetic field.

Figure 3.12 -see Appendix A- shows a plot of the magnetization as a function of the magnetic field at temperature T=0.1K, and five different values of SOI-parameters α_R (0,40,50,60, 70 *meV* nm), and Dresselhaus β_D (0, 20,25,30,35 *meV* .nm). the copmuted results show that all peaks of M -curve are shifted to the left. This comparable to Figure 3.10 results means that the peaks appear clearly at lower values of magnetic field B as we include the Rashba and Dresselhaus terms. At α_R = 40 *meV*. nm and β_D=20 *meV* .nm values, M decreases as B increases up to B~0.72T where the first peak appear and the

magnetization then continues increasing up to reach the second peak at B$\sim 0.86T$,then M returns to decrease again with increasing of the magnetic field.

At higher SOI-parameters, α_R = 50 *meV*. nm and β_D=25 *meV*. nm, the first downward peak appears at B $\sim 2.007T$ then M start to increase up to reach the second peak at B$\sim 2.08T$ and returns to decrease again. Stronger case: at α_R = 60 *meV*. nm and β_D=30 *meV* .nm, the first downward peak occurs at B$\sim 3.33T$ and M goes to increase up to the second peak at B$\sim 3.41T$ and becomes decreasing again. At α_R = 70 *meV*. nm and β_D=35 *meV* .nm, the first peak of the curve occurs at B$\sim 4.73T$ and the path went up to the second peak at b$\sim 4.8T$, then return to decrease again. All the M-curves decrease to converge up to approximately a stable of magnetization value $M \sim 0.699$, which remains approximately constant as the value of the magnetic field increases.

Figure 3.13 -see Appendix A- shows a plot of the magnetization M as a function of B(T) now at high temperature T= 10(K),range with five different values of Rashba and Dresselhaus parameters (α_R = 0, 40,50,60 & 70 *meV* .nm, β_D = 0,20,25,30 & 35 *meV* .nm). All peaks at high T are disappeared due to thermal effect ($E_{th} \approx k_\beta T$), and the magnetization curves are shift down.

Figure 3.14 -see Appendix A- shows the Susceptibility plot of InAs-QWW material as a function of magnetic field at certain value of temperature T=0.1K and four different values of Rashba SOI parameter α_R (0,40, 50 & 60 *meV* nm) with Dresselhaus effect $\beta_D = 0$ firstly. For all curves with $\alpha_R \geq 40\, mev.nm$ the graph shows clearly the oscillation behaver of χ from negative (Diamagnetic $\chi < 0$) to positive (Paramagnetic$\chi > 0$). At α_R = 40 *meV* nm, χ change its behavior from negative to positive at B $\sim 1.56T$ and then its change from positive to negative again at B$\sim 1.67T$. at α_R =50 *meV*. nm, χ change from negative to positive at B$\sim 3.02T$,and returns from positive to negative at B$\sim 3.12T$, finally at α_R =60 *meV*. nm susceptibility changes the sign from negative to positive at B $\sim 4.6T$ and return changes from positive to negative value at B$\sim 4.73T$. These peaks appears at certain values of B where there is oscillations.

These values of magnetic field at which the sign of the Susceptibility (χ) changes match and equal to the corresponding values of B in the magnetization (M) curve. The peaks appear indicates a magnetic change in phase a QWW made from InAs- material.

To investigate the effect of α_R on the magnetic phase transition, we have shown in Figure 3.15, -see Appendix A- the Susceptibility as a function of magnetic field at temperature T= 10 K for five different values of α_R (0, 40,50,60,70 *meV* nm). Its clear from the graphs that all the peaks are disappeared, while the values of χ-curves changes from negative to positive. At α_R = 40 *meV* nm the curve of χ changes its sign form diamagnetic ($\chi < 0$) material to paramagnetic ($\chi > 0$) material as we increase the strength of the magnetic field. The magnetic phase transition in the $\chi -$ curve can be observed at different values of B as we change α_R- parameter. The calculations shows clearly that an important effective for Rashba factor α_R in controlling the magnetic of QWW- material type.

Figure 3.16 -see Appendix A- shows a plot of Susceptibility χ as a function of magnetic field B(T) at temperature T=0.1K and five different values of Rashba parameters α_R(0,40,50,60 & 70 *meV*.nm) and five different values of Dresselhaus parameters β_D (0, 20,25,30 & 35 *me*. nm). The χ-curve shows an obvious peak occurs at α_R =40 *meV*.nm and β_D= 20 *meV*.nm, from the curve, χ firstly has a negative value and this value increases negatively up to B$\sim 0.72T$ then χ become decrease negatively until it become has a positive value and become increase positively up to B$\sim 0{,}84T$ then χ return to decrease and change the sign again.. Note that all curves after the peaks are meet at approximately similar value of susceptibility although the strength of magnetic field increases. At low T=0.1K, the peaks in the $\chi - curve$ become pronounced and very clear at high negative values as the strength of α_R and β_D become very strong because these effects together.

Figure 3.17 -see Appendix A- shows χ-curve as a function of magnetic field at temperature T= 10 K and five different values of α_R (0,40,50,60&70 *meV*. nm) and five different values of $\beta_D = \frac{1}{2}\alpha_R$., The plot shows that all peaks in the χ-curves disappeared at T=10K and various magnetic phase changes are observed compared with the case T=0.1K.

3.4 The Effect of Transverse Confining Potential strength on the Magnetization and Susceptibility of InAs-QWW

In this section, we present and describe the effects of Transverse Hamiltonian ($\widehat{H}_{SO}^{T}$) $given\ by\ Eq.2.3$ on M and χ. As we vary the strength of the SO coupling parameter γ.

Firstly, we study the effect of γ on the Average energy at $\alpha_R = \beta_D = 0$ meV nm and T =0.1K. From Figure 3.18.a -see Appendix A- at $\gamma = 1\ and\ 4\ meV.nm$, we see the effect of γ is marginal and the shift of the curve of the average energy as a function of B very small that means the transverse effect very week compared with Rashba and Dresselhaus effects but it has a value. Figure 3.18.b -see Appendix A- shows a plot of Average energy as a function of B at high temperature T = 10K and $\gamma = 1\ and\ 4\ meV\ nm$, with $\alpha_R = 0$ and$\beta_D = 0$, the shifting up of the curves and the splitting of states becomes larger than at T=0.1K due to the thermal effect.

Figure 3.19.a -see Appendix A- shows average energy curve as a function of magnetic field (B) at T=0.1K with two different values of γ=1 and 4 $meV.nm$ with Rashba parameter α_R= 40 meV.nm and Dresselhaus parameter β_D=20 meV. nm. These three effects together at low temperature with change the values of B Shift the curve of average energy downwards, but the shift is marginal. At T=10 K the shift of the curve becomes a little bigger compared to the shift at T=0.1k as shown in Figure 3.19.b -see Appendix A- i.e., the transverse effect is very weak but exists and become stronger with Rashba and Dresselhaus at certain value of temperature.

Figure 3.20.a -see Appendix A- shows a plot of magnetization M as a function of magnetic field of InAs-QWW material under transverese effect at low temperature T=0.1K and with $\alpha_R = 0\ meV.nm$ and $\beta_D = 0meV.nm$. We take two values of $\gamma = 1\ and\ 4\ meV.nm$. From the graph we see that the curve of M shifts up when γ increase but the shift very week. Figure 3.20.b -see Appendix A- shows the plot of magnetization with respect to B but at T=10K, the main difference between two graphs is the shifting of the curves becomes larger becouse of the effect of T on the energy ststes i.e. it shift the energy ststes up so the effect of transverese parameter become stronger with T.

Figure 3.21.a -see Appendix A- shows M as a function of B under two values of transverse factor $\gamma = 1$ & $4\ meV\ nm$ at T=0.1K with Rashba and Dressalhouse effects and we take α_R = 40 meV .nm and β_D = 20 meV .nm. From the graph at $\gamma = 1\ meVnm$ we got a small peak and it orianted downward at B = 0.65 T and $M = -0.25$ then the curve change the direction upward and another peak apeare but it orianted upward at B=0.79 T and $M = -0.23$. If we compear these peaks with the peaks of the curve of magnetization as a

function of B in Figure 3.12 at $\gamma = 0$, α_R = 40 mev nm and β_D = 20 mev nm, we see that the first downward peak appears at B= 0.72 T and $M = -0.29$ and the second upward peak apears at B =0.86 T and $M = -0.24$, we concloude that the peaks with transverese effect shift to the left and need lower values of magnetic field to apear which means that the transverese effect is week compeared with Rashba and Dresselhaus effects.

Figure 3.21.b -see Appendix A- represents the plot of magnetization as a function of magnetic field at high T=10 K and same two different values of γ=1 &4 meV nm, with, α_R = 40 $meV\ nm$ and β_D = 20 $meV\ nm$, all peaks are dissapear and the shape of the curve start increase and M positve in two curves up to B~$0.37T$ then the two curves of magnetization becomes decrease and take negative values up to B~$3.5T$ and the two curves return to moves upward again but M remains negative. If we compare this graph with Figure 3.13 at α_R = 40 meV. nm and β_D = 20meV. nm, we see the value of M starts decreasing up to B~$0.9T$ then increases shortly up to B~$1.6T$, then reterns to decrease again and all values of M are negative, but when we take the trenseverse parmeter into account the values of M switches (turns) from possitive to negative, that means This means that the presence of a transverse confinement potintial affects magnetization of InAs-QWW material from the diamagnetic to paramagnetic, and this is what we want to control of the magnetic behavior of InAs- material.

After the magnetization we study the effect of γ on susceptibility χ, firstly we take the teansverse factor alone at T=0.1 K as shown on Figure 3.22 -see Appendix A- and we take again two values of $\gamma = 1\ and\ 4\ meV.nm$. From graph we see the values of χ increase as B values increase but all values remain negative in two values of γ. But the curve have marginal shift up when $\gamma = 4\ meV.nm$.

Figure 3.23.a -see Appendix A- shows a plot of X as a function of B (T) at low temperature T=0.1K and the three effects (Rashba, Dresselhaus and Transvese effects) with α_R = 40 meV. nm, β_D = 20meV. nm and $\gamma = 1\ and\ 4\ meV.nm$. We see firstly at $\gamma = 1\ meV.nm$ the peaks apear in the curve, firstly χ start decrease up to B~$0.3\ T$ and the minimum value of $\chi \sim -0.39$,then the curve moves upward to receave a peak at B~$0.55T$ and $\chi = -0.013$ then the curve retern to decrease up to B~$0.77T$ and $\chi = -0.35$ and become to inrease when B increas linearly. If we compaire this curve with Figure 3.16 at α_R = 40

meV. nm, $\beta_D = 20meV$. nm, the peak apear at B$\sim 0.84T$, and χ =0.35, so when γ occure we get the peak with lower value of B. i.e. three effects togather they are more powerful than the external magnetic field. At $\gamma = 4\ meV.nm$, the curve similarly start decreasing up to B$\sim 0.48T\ and\ \chi = -0.52$ then it becomes increase and a peak occure at B$\sim 0.72T\ and\ \chi = 0.25$ then the curve return to decrease fastly up to B$\sim 0.88T$ then χ return to increase linearly with B increase. Note that when γ increase the peak shift to the right but the maximum value of χ is larger.

Figure 3.23.b -see Appendix A- shows a plot of χas a function of B at high T=10 K, from graph we see the two curves start ro decrease up to B$\sim 0.8T$ with $\chi \sim -0.39\ at\ \gamma = 1\ meV.nm\ and\ \chi = -0.40\ at\ \gamma - 4\ meV.nm$, then the two curves start to increase again up to B$\sim 3.12\ T$ with $\chi = 0.024\ at\ \gamma = 4\ meV.nm\ and\ at\ \gamma = 1\ meV.nm\ \chi = 0.11$ then *X* return to decrease again and return to be negative.

When we compare the curves with Figure 3.17 we see the same behavior of the curves.

Chapter Four

Conclusions

In this work, we have studied the magnetic properties of quantum well wire system by computing the magnetization (M) and susceptibility (χ) . The Hamiltonian of QWW for 1D InAs heterostructure has been solved by using exact diagonalization method. We obtained the eigenvalues of energy spectra under magnetic field, Rashba effect, Zeeman effect, Dresselhaus effect and Transverse confinement potential .

In addition, we have used the energy eigenvalues to calculate the average energy for the system for different subbands. We focus on the effect of Rashba term on average energy as a function of temperature at certain value of magnetic field. We have taken the Rashba and Dresselhaus combined effects at certain magnetic field values and we calculate the average energy as a function ot temperature. The average energy as a function of magnetic field under Rashba has been investigated firstly, then with Rashba and Dresselhaus together at temperature range T(0.1,10K).

We have shown the dependence of the magnetic properties, magnetization and susceptibility as a function of magnetic field under Rashba effect and at temperature limits. Farthemore,we have studied M & χ under two joined effects i.e, Rashba and Dresselhaus at low and high T.

Taking the Transverse confinement potential into account, and we computed the average energy under transverese confinement effect and magnetic field, then we add Rashba and Dresselhaus to Transeverse confinement poteintial and magenetic field. The calculations shows clearly that the Rashba parameter shifts the cuves of average energy at low and high B limits and these shifts become larger when temperature increases. When Rashaba and Dresselhaus included together the level of degeneracy removed at low and high B and T limits. As we switch on α_R, we control strongly the magnetic properties of InAs-QWW (Magnetization and Susceptibility) . Dresselhaus parameter controls the magnetic prperties too but weakly than Rashba parameter. The Transverse confineing potential has a marginal effect on magentization and susceptibility of InAs-QWW material.

List of Abbreviations

D_f	Number of degrees of freedom
D_c	Number of directions of quantum confinement
QD	Quantum Dot
QW	Quantum Well
QWW	Quantum Well Wire
3D	Three Dimensions
2D	Two Dimensions
1D	One Dimension
0D	Zero Dimension
InAs	Indium Arsenide
GaAs	Gallium Arsenide
K	Wave vector
2DEG	Two dimensional electron gas
SOI	Spin Orbit Interaction
DOS	Density Of States
M	Magnetization
χ	Susceptibility
$\boldsymbol{k}$	Wave vector
H	Hamiltonian
α_R	Rashba parameter
$\boldsymbol{P}$	Momentum operator
$\boldsymbol{\sigma}$	Pauli matrices
E_n	Energy spectrum
$\hbar$	Reduced Blank constant
$\langle E \rangle$	Average statistical energy
m_0	Rest mass of electron
m^*	Effective mass of electron
$\boldsymbol{A}$	Magnetic vector potential
$\boldsymbol{B}$	Magnetic field
H_R	Rashba Hamiltonian
e	Electron charge
ω_0	Frequency of confinement potential
ω_c	Cyclotron frequency
ω	Effective cyclotron frequency
ħ	Reduced Blank's constant
a^*	Effective Bohr radius
H_D	Dresselhaus Hamiltonian

β_D	Dresselhaus parameter
meV	milli electron Volt
nm	Nanometer
k_B	Boltzmann constant
g^*	Effective Lande factor of the electron
T	Temperature
K	Kelvin degree
μ_B	Bohr $Magneton$
c	Speed of light
H_{SO}^T	Hamiltonian $of\ SOI$
γ	Spin orbit coupling parameter
l_0	l$ength\ scale$

Referances

[1] Hornyak, G. L., Moore, J. J., Tibbals, H. F., & Dutta, J. (2018). Fundamentals of nanotechnology. CRC press.

[2] Al Thaher, Y., Satoof, A., Kamal, A., Almani, D., Shaban, D., Kassab, G., ... & Ajaleh, S. A. (2021). Instrumental analytical techniques for physicochemical characterization of bio-nanomaterials. In *Handbook on Nanobiomaterials for Therapeutics and Diagnostic Applications* (pp. 133-150). Elsevier.

[3] Azmi, M. A., & Shad, K. F. (2017). Role of nanostructure molecules in enhancing the bioavailability of oral drugs. In Nanostructures for novel therapy (pp. 375-407). Elsevier.

[4] Henini, M. (Ed.). (2011). Handbook of self-assembled semiconductor nanostructures for novel devices in photonics and electronics. Elsevier.

[5] Shaer, A., ELSAID, M., & Elhasan, M. (2016). The magnetic properties of a quantum dot in a magnetic field. Turkish Journal of Physics, 40(3), 209-218.

[6] Martin, P. M., Olsen, L. C., Bennett, W. D., & Henager, C. H. (2006). Superlattice Coatings for Device, Structural and Protective Applications (No. PNNL-SA-51747). Pacific Northwest National Lab. (PNNL), Richland, WA (United States).

[7] Liang, D., & Gao, X. P. (2012). Strong tuning of Rashba spin–orbit interaction in single InAs nanowires. Nano Letters, 12(6), 3263-3267.

[8] Vaseghi, B., & Ghaffari, A. (2016). Effects of spin–orbit interaction on the electronic structure of mono-layer quantum wires. Physica E: Low-dimensional Systems and Nanostructures, 81, 163-168.

[9] Sarma, S. D. (2001). Spintronics: A new class of device based on electron spin, rather than on charge, may yield the next generation of microelectronics. American Scientist, 89(6), 516-523.

[10] Pingale, J. S., Patil, M. D., & Masumdar, U. I. (2013). Utilization of Spintronics. International Journal of Scientific and Research Publications, 614.

[11] Žutić, I., Fabian, J., & Sarma, S. D. (2004). Spintronics: Fundamentals and applications. Reviews of modern physics, 76(2), 323.

[12] Yin, Y. (2018). Spin-orbitronics: novel interactions and magnetoresistances in ultrathin magnetic films.

[13] Boda, A., Boyacioglu, B., Erkaslan, U., & Chatterjee, A. (2016). Effect of Rashba spin–orbit coupling on the electronic, thermodynamic, magnetic and transport properties of GaAs, InAs and InSb quantum dots with Gaussian confinement. *Physica B: Condensed Matter*, *498*, 43-48.

[14] Ali, A. A., Shaer, A., & Elsaid, M. (2022). Simultaneous effects of Rashba, magnetic field and impurity on the magnetization and magnetic susceptibility of a GaAs-semiconductor quantum ring. *Journal of Magnetism and Magnetic Materials*, *556*, 169435.

[15] Lesne, E., Fu, Y., Oyarzun, S., Rojas-Sánchez, J. C., Vaz, D. C., Naganuma, H., & Vila, L. (2016). Highly efficient and tunable spin-to-charge conversion through Rashba coupling at oxide interfaces. Nature materials, 15(12), 1261-1266.

[16] Manchon, A., Koo, H. C., Nitta, J., Frolov, S. M., & Duine, R. A. (2015). New perspectives for Rashba spin–orbit coupling. Nature materials, 14(9), 871-882.

[17] Liang, D., & Gao, X. P. (2012). Strong tuning of Rashba spin–orbit interaction in single InAs nanowires. Nano Letters, 12(6), 3263-3267.

[18] Dresselhaus, G. (1955). Spin-orbit coupling effects in zinc blende structures. Physical Review, 100(2), 580.

[19] Zhang, T. Y., Zhao, W., & Liu, X. M. (2009). Energy dispersion of the electrosubbands in parabolic confining quantum wires: interplay of Rashba, Dresselhaus, lateral spin–orbit interaction and the Zeeman**.** effect. Journal of Physics: Condensed Matter, 21(33), 335501.

[20] Malik, G. F. A., Kharadi, M. A., Khanday, F. A., & Parveen, N. (2020). Spin field effect transistors and their applications: A survey. *Microelectronics Journal*, *106*, 104924

[21] Frolov, S. M., Plissard, S. R., Nadj-Perge, S., Kouwenhoven, L. P., & Bakkers, E. P. (2013). Quantum computing based on semiconductor nanowires. *MRS bulletin*, *38*(10), 809-815.

[22] Laucht, A., Hohls, F., Ubbelohde, N., Gonzalez-Zalba, M. F., Reilly, D. J., Stobbe, S., ... & Baugh, J. (2021). Roadmap on quantum nanotechnologies. *Nanotechnology*, *32*(16), 162003.

[23] Liu, J. F., Zhong, Z. C., Chen, L., Li, D., Zhang, C., & Ma, Z. (2007). Enhancement of polarization in a spin-orbit coupling quantum wire with a constriction. Physical Review B, 76(19), 195304.

[24] Chen, L., Ma, Z., Cao, J. C., Zhang, T. Y., & Zhang, C. (2007). Phonon-limited mobility in two-dimensional semiconductors with spin-orbit coupling. Applied Physics Letters, 91(10), 102115.

[25] Elsaid, M. K., & Hijaz, E. (2017). Magnetic Susceptibility of Coupled Double GaAs Quantum Dot in Magnetic Fields. *Acta Physica Polonica, A.*, *131*(6).

[26] Bychkov, Y. A. (1984). Properties of 2D electron gas with lifted spectral degeneracy. JETP lett., 39(2), 78-81.

[27] Elsaid, M. K., Alia, A. A., & Shaer, A. (2020). Rashba spin-orbit interaction effects on thermal and magnetic properties of parabolic GaAs quantum dot in the presence of donor impurity under external electric and magnetic fields. *Chinese Journal of Physics*, *66*, 335-348.

[28] Malet, F., Lipparini, E., Barranco, M., & Pi, M. (2006). Spin-orbit effects on the Larmor dispersion relation in GaAs quantum wells. Physical Review B, 73(12), 125302.

[29] Bliokh, K. Y., Rodríguez-Fortuño, F. J., Nori, F., & Zayats, A. V. (2015). Spin–orbit interactions of light. *Nature Photonics*, *9*(12), 796-808.

[30] Ho, T. L., & Zhang, S. (2011). Bose-Einstein condensates with spin-orbit interaction. *Physical review letters*, *107*(15), 150403.

[31] Bihlmayer, G., Koroteev, Y. M., Echenique, P. M., Chulkov, E. V., & Blügel, S. (2006). The Rashba-effect at metallic surfaces. *surface science*, *600*(18), 3888-3891.

[32] Rajab, H. S. (2021). *The Effects of Rashba Spin-orbit Interaction and Magnetic Field on the Thermo-Magnetic Properties of an Electron Confined in a Cylindrical Semiconductor Quantum Dot* (Doctoral dissertation, جامعة النجاح الوطنية).

[33] Bejan, D., Stan, C., & PETRESCU-NIȚĂ, A. (2022). MAGNETIC PROPERTIES OF PSEUDO-ELLIPTIC QUANTUM RINGS: INFLUENCE OF IMPURITY POSITION AND ELECTRON SPIN. *UNIVERSITY POLITEHNICA OF BUCHAREST SCIENTIFIC BULLETIN-SERIES A-APPLIED MATHEMATICS AND PHYSICS*, *84*(1), 163-174.

[34] Wang, W. T., Wu, C. L., Tsay, S. F., Gau, M. H., Lo, I., Kao, H. F., ... & Hsueh, H. C. (2007). Dresselhaus effect in bulk wurtzite materials. *Applied Physics Letters*, *91*(8), 082110.

[35] El-Said, M. (1994). The magnetoabsorption spectra of donors in a quantum well wire. *Semiconductor science and technology*, *9*(10), 1787.

[36] Elsaid, M. K., & Hijaz, E. (2017). Magnetic Susceptibility of Coupled Double GaAs Quantum Dot in Magnetic Fields. Acta Physica Polonica, A., 131(6).

[37] Elsaid, M. K., Alia, A. A., & Shaer, A. (2020). Rashba spin-orbit interaction effects on thermal and magnetic properties of parabolic GaAs quantum dot in the presence of donor impurity under external electric and magnetic fields. Chinese Journal of Physics, 66, 335-348.

[38] Shaer, A., Elsaid, M. K., & Elhasan, M. (2016). Magnetization of GaAs parabolic quantum dot by variation method. *J. Phys. Sci. Appl*, *6*(2), 39-46.

[39] Hjaz, E., Elsaid, M. K., & Elhasan, M. (2017). Magnetization of coupled double quantum dot in magnetic fields. Journal of Computational and Theoretical Nanoscience, 14(4), 1700-1705.

[40] Alia, A. A., Elsaid, M. K., & Shaer, A. (2019). Magnetic properties of GaAs parabolic quantum dot in the presence of donor impurity under the influence of external tilted electric and magnetic fields. Journal of Taibah University for Science, 13(1), 687-695.

[41] Dhara, S., Solanki, H. S., Singh, V., Narayanan, A., Chaudhari, P., Gokhale, M., ... & Deshmukh, M. M. (2009). Magnetotransport properties of individual InAs nanowires. Physical Review B, 79(12), 121311.

[42] Blömers, C., Lepsa, M. I., Luysberg, M., Grutzmacher, D., Luth, H., & Schapers, T. (2011). Electronic phase coherence in InAs nanowires. Nano letters, 11(9), 3550-3556.

[43] Perla, P., Fonseka, H. A., Zellekens, P., Deacon, R., Han, Y., Kölzer, J., ... & Schäpers, T. (2021). Fully in situ Nb/InAs-nanowire Josephson junctions by selective-area growth and shadow evaporation. Nanoscale Advances, 3(5), 1413-1421.

[44] Bzour, F., Elsaid, M. K., & Shaer, A. (2017). The effects of pressure and temperature on the magnetic susceptibility of semiconductor quantum dot in a magnetic field. *App. Phys. Res*, *9*, 77-82.

[45] Alia, A. A., Elsaid, M. K., & Shaer, A. (2019). Magnetic properties of GaAs parabolic quantum dot in the presence of donor impurity under the influence of external tilted electric and magnetic fields. *Journal of Taibah University for Science*, *13*(1), 687-695

[46] راشد شتيوي, & ضحى. (2020). *Effects of Exchange Energy and Rashba Terms on the Magnetic Properties of A Diluted Hg1-xMnxTe Semiconductor Quantum Dot* (Doctoral dissertation, جامعة النجاح الوطنية).

[47] Yaseen, A., Shaer, A., & Elsaid, M. K. (2019). The magnetic properties of GaAs parabolic quantum dot in the presence of donor impurity, magnetic and electric fields. *Chinese Journal of Physics*, *60*, 598-611.

[48] عيسى مغربي, & أمامه. (2021). THE MAGNETIZATION AND MAGNETIC SUSCEPTIBILITY OF AN ELECTRON CONFINED IN A DOPED QUANTUM RING MADE OF GAAS/ALGAAS IN A MAGNETIC FIELD (Doctoral dissertation, جامعة النجاح الوطنية).

[49] Kirak, M. U. H. A. R. R. E. M., Altinok, Y., & Yilmaz, S. A. İ. T. (2013). The effects of the hydrostatic pressure and temperature on binding energy and optical properties of a donor impurity in a spherical quantum dot under external electric field. *Journal of Luminescence*, *136*, 415-421.

[50] Mehta, R. C., Pike, G. B., & Enzmann, D. R. (1996). Magnetization transfer magnetic resonance imaging: a clinical review. *Topics in magnetic resonance imaging*, *8*(4), 214-230.

[51] Voskoboynikov, O., Bauga, O., Lee, C. P., & Tretyak, O. (2003). Magnetic properties of parabolic quantum dots in the presence of the spin–orbit interaction. *Journal of applied physics*, *94*(9), 5891-5895.

[52] Elsaid, M. K., Shaer, A., Hjaz, E., & Yahya, M. H. (2020). Impurity effects on the magnetization and magnetic susceptibility of an electron confined in a quantum ring under the presence of an external magnetic field. *Chinese Journal of Physics*, *64*, 9-17.

[53] Tangarife, E., & Duque, C. A. (2010). Combined effects of hydrostatic pressure and electric field on the donor binding energy and polarizability in laterally coupled double InAs/GaAs quantum-well wires. *Applied surface science*, *256*(23), 7234-7241.

Appendices

Appendix A

Figure

Figure 3.7.b

Average Energy versus T at B=1T.

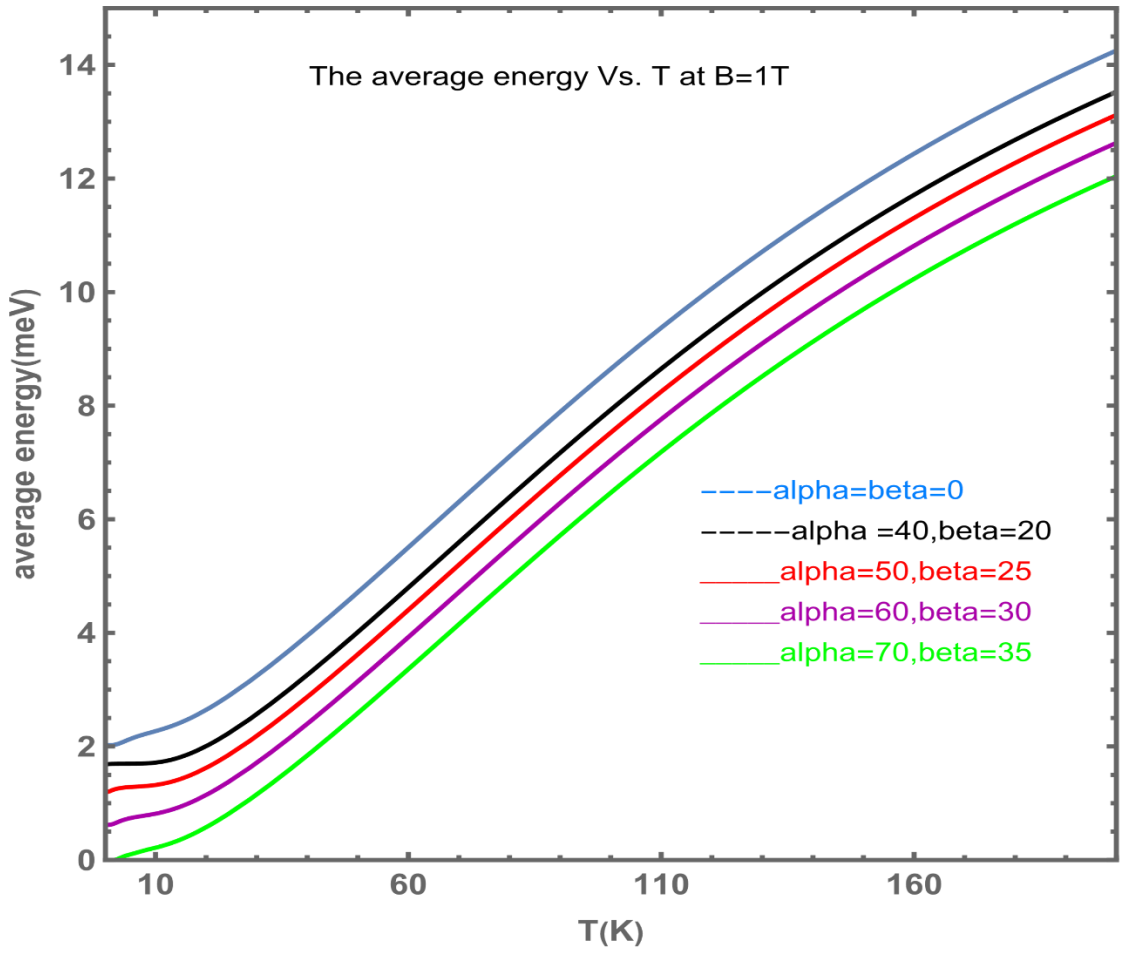

Figure 3.8.a

Average energy against. B(T) at T=0.1K and β= 0 meV. nm

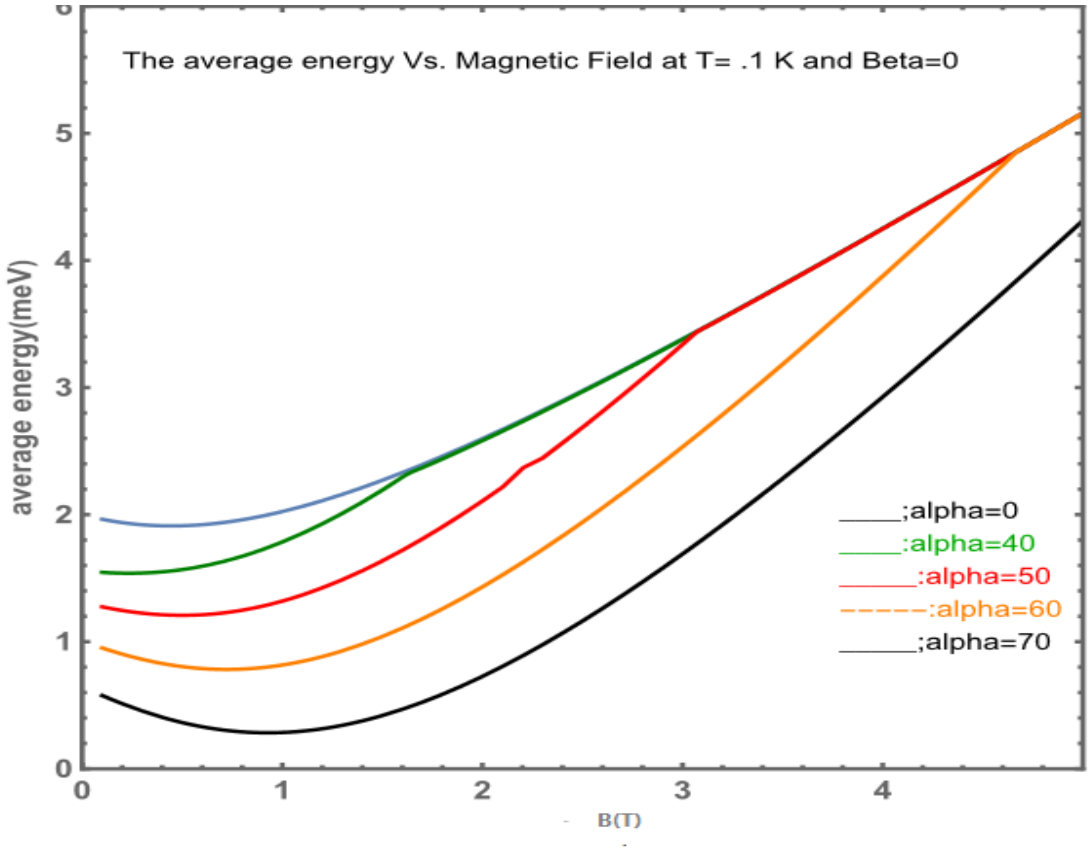

Figure 3.8. b

Average Energy as a function of B(T) at T=10K and β_D=0 meV.nm

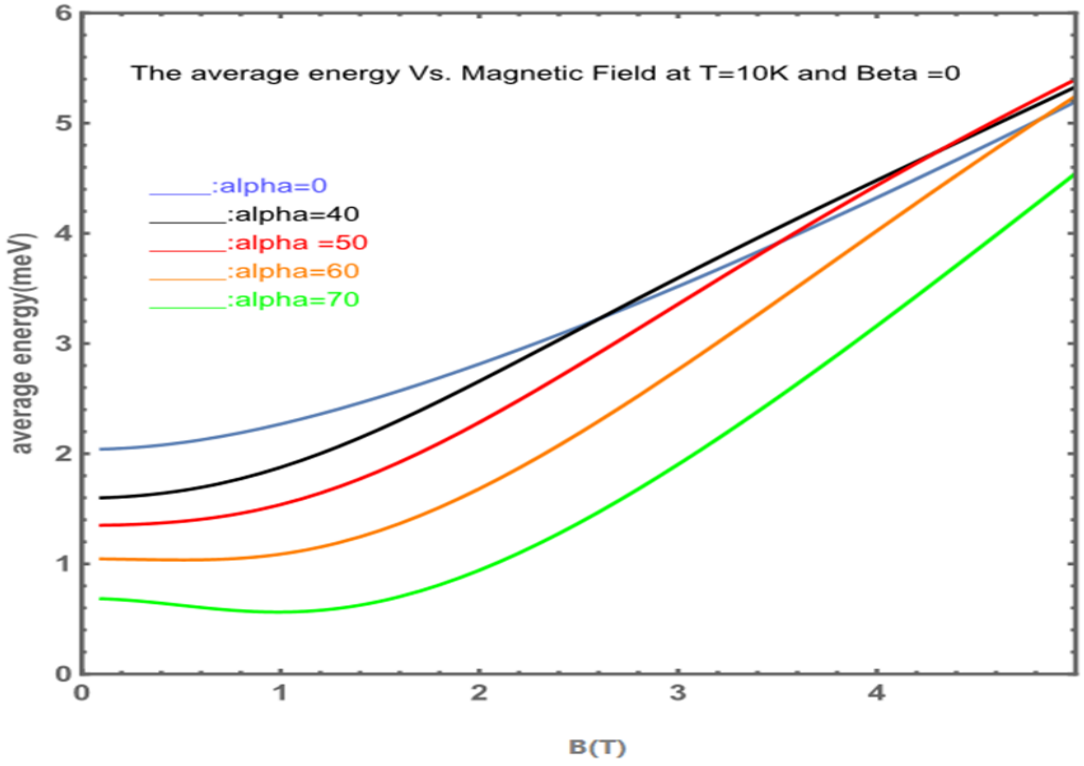

Figure 3.9.a

Average Energy versus B at T =0.1K.

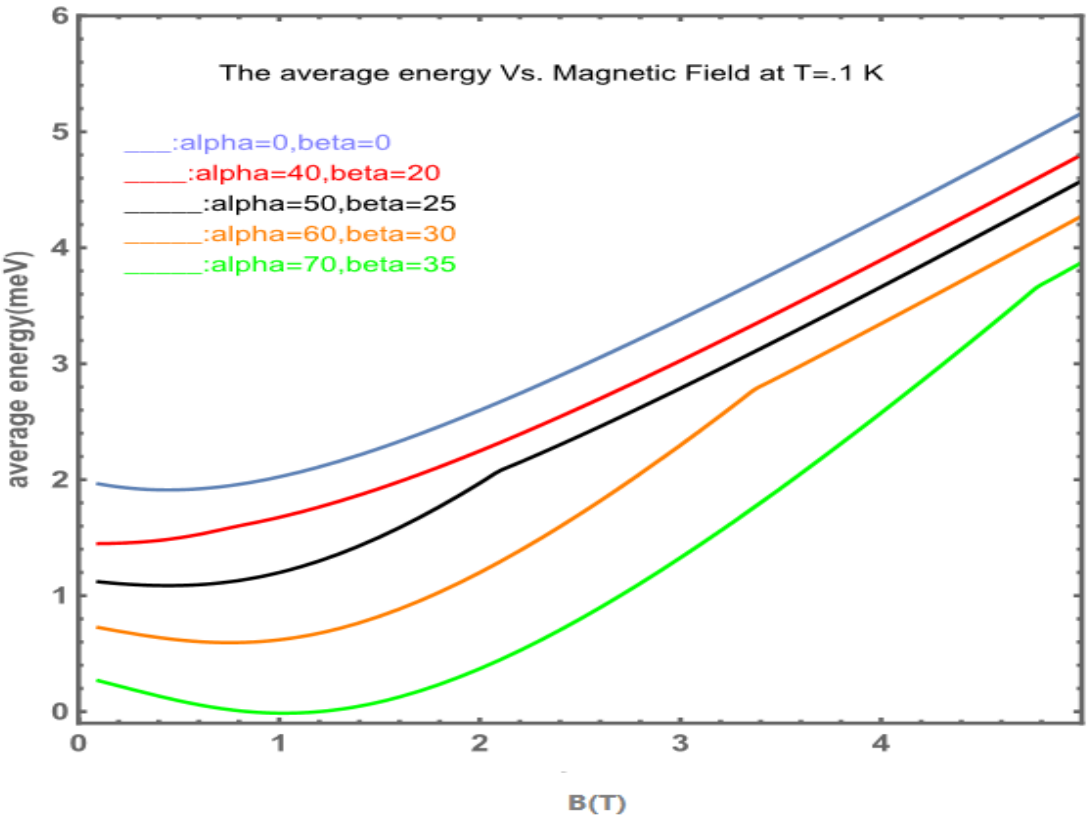

Figure 3.9.b

Average Energy versus B (T) at T=10 K

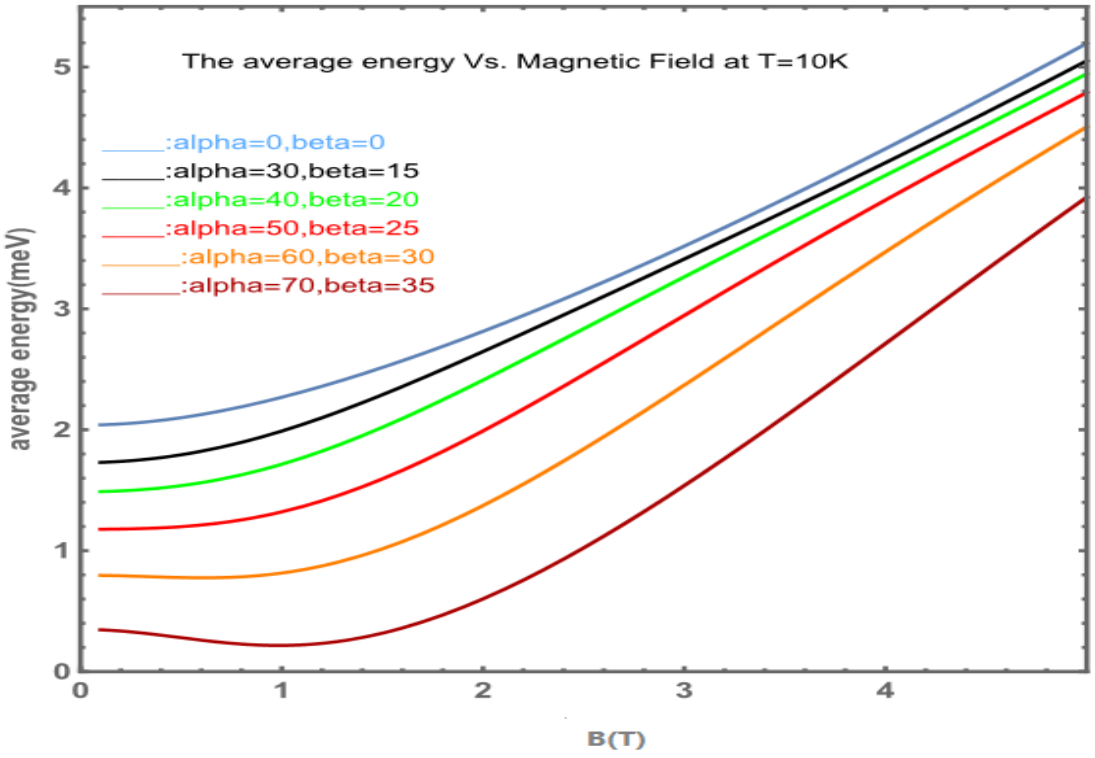

Figure 3.10

Magnetization against B at β_D =0 meV .nm and T=0.1K at different values of α_R.

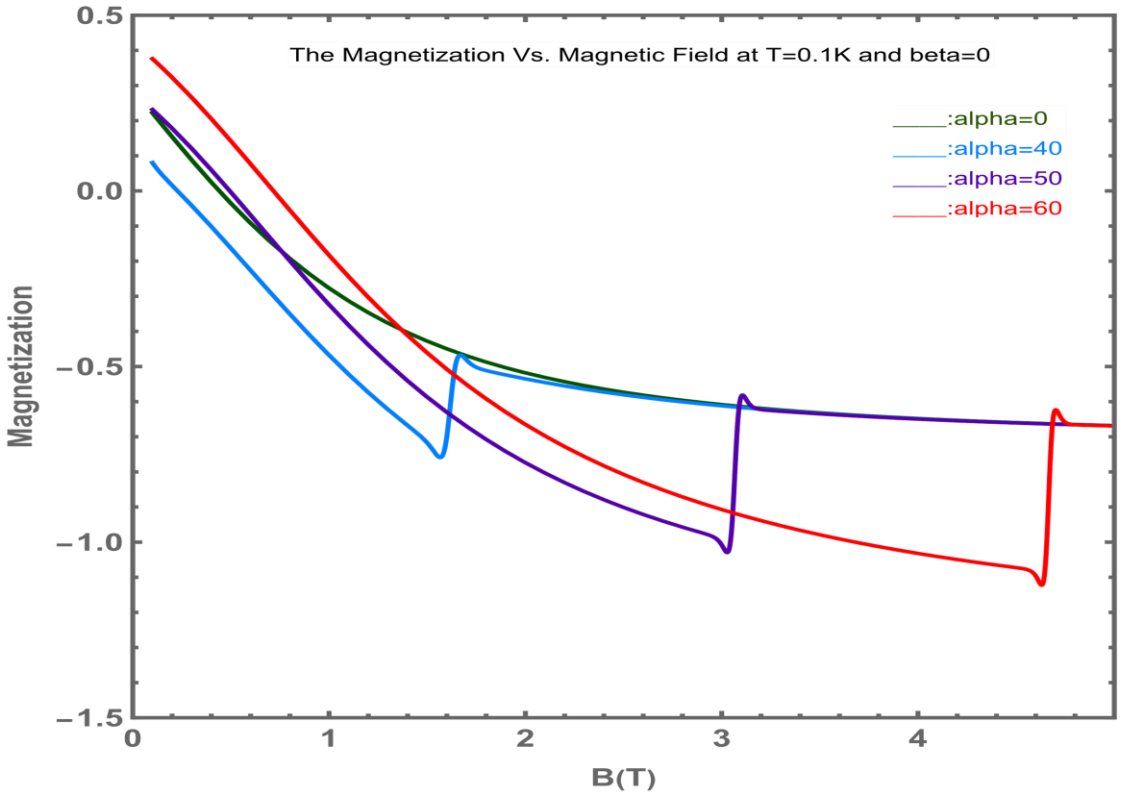

Figure 3.11

Magnetization against B(T) at T=10K and β_D = 0 meV. nm with four different values of α_R.

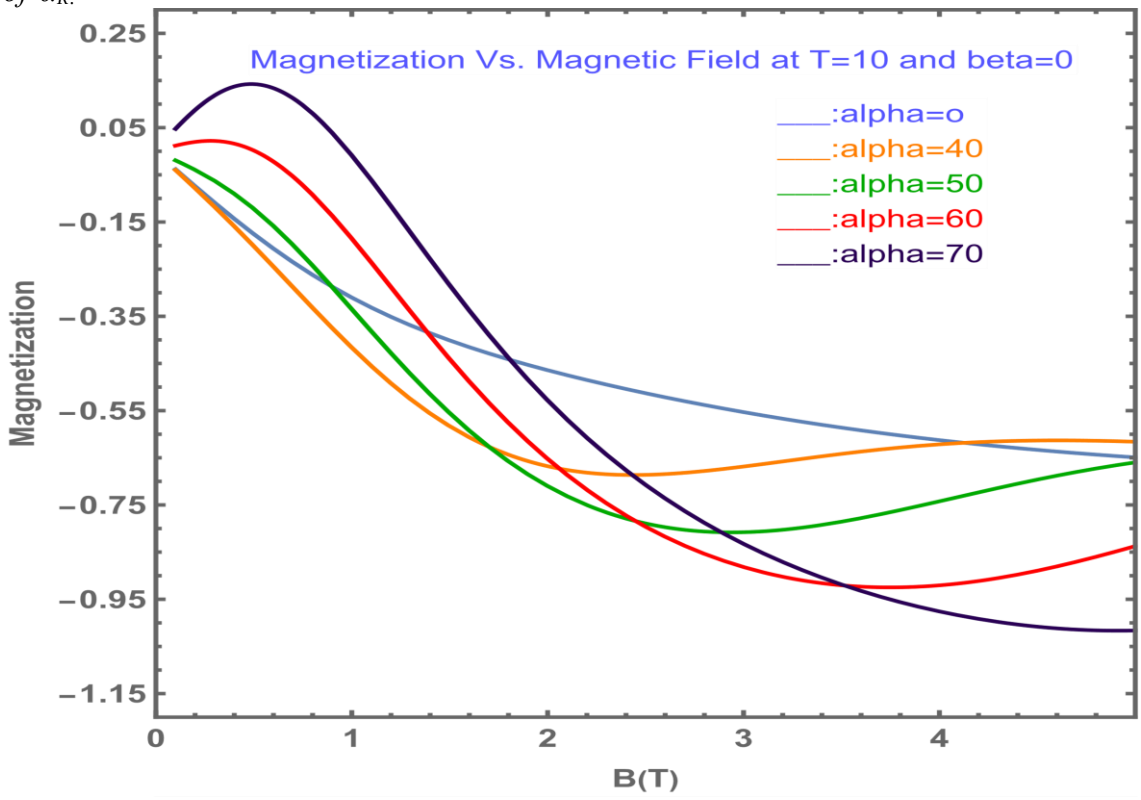

Figure 3.12

Magnetization against B(T) at T=0.1K, and five different values of α_R and β_D.

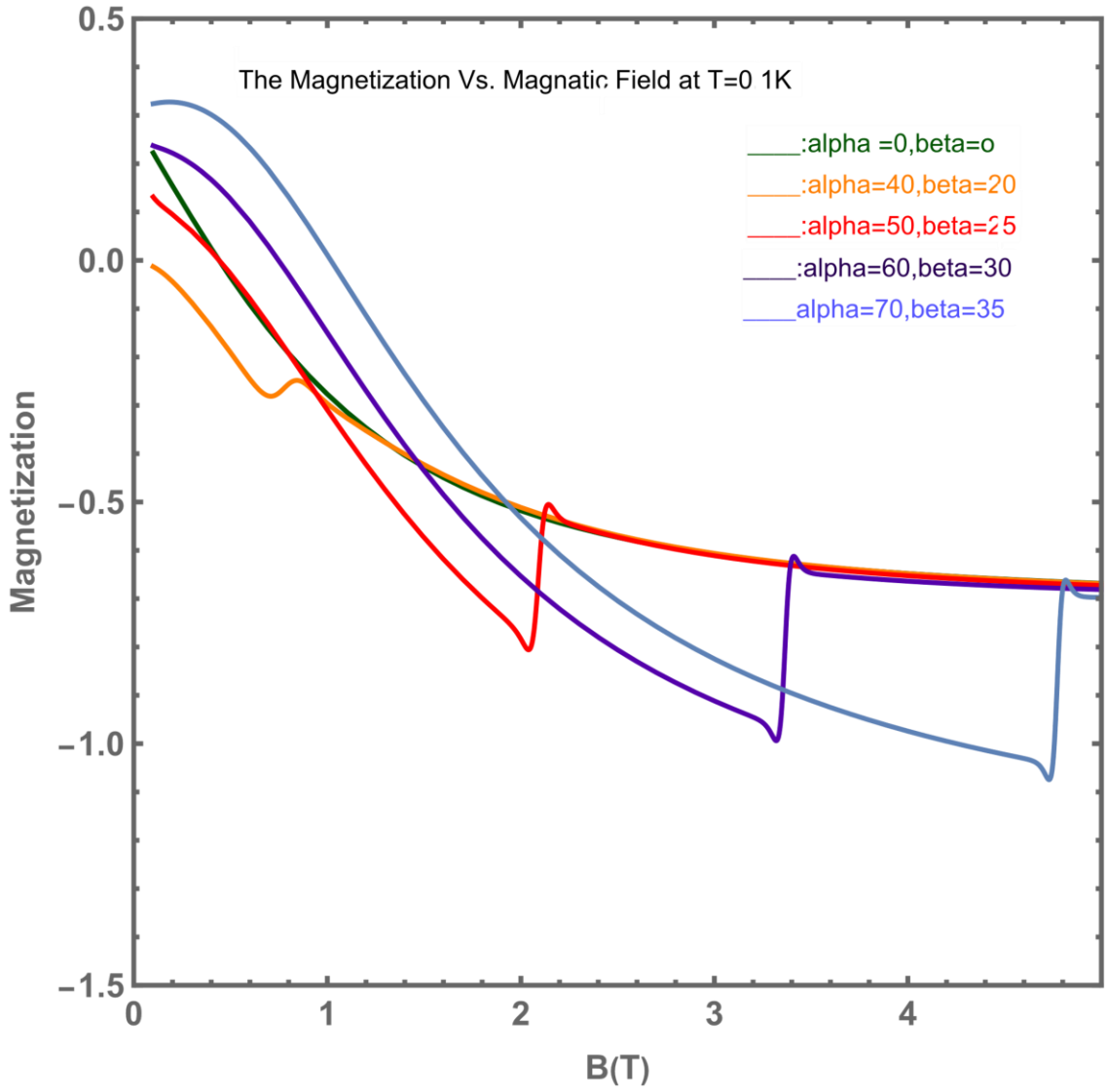

Figure 3.13

Magnetization against B(T) at T= 10 K and five different values of α_R and β_D.

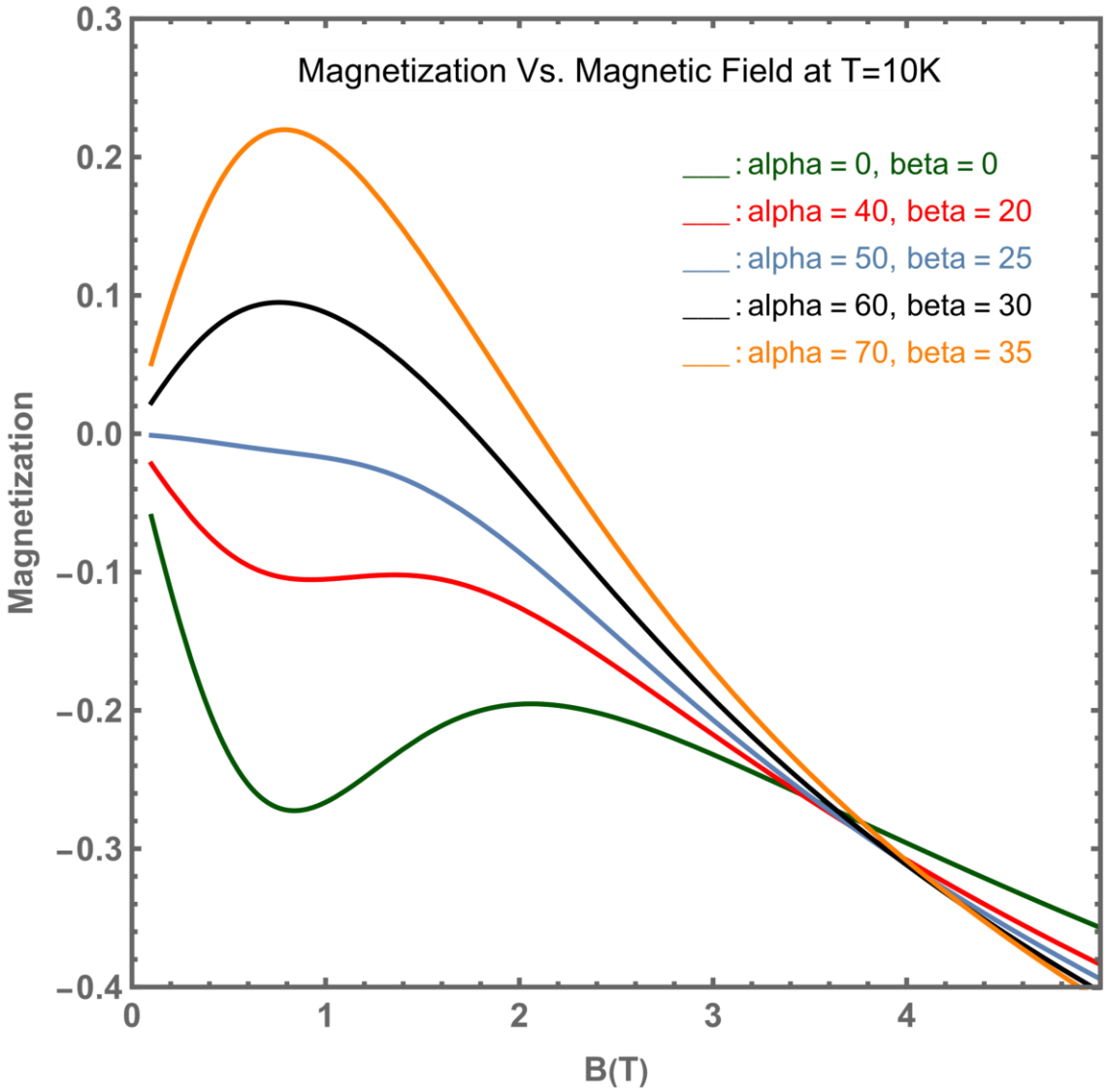

Figure 3.14

Susceptibility as a function of B(T) at T= 0.1 K and β_D=0 meV nm and diferent values of α_R.

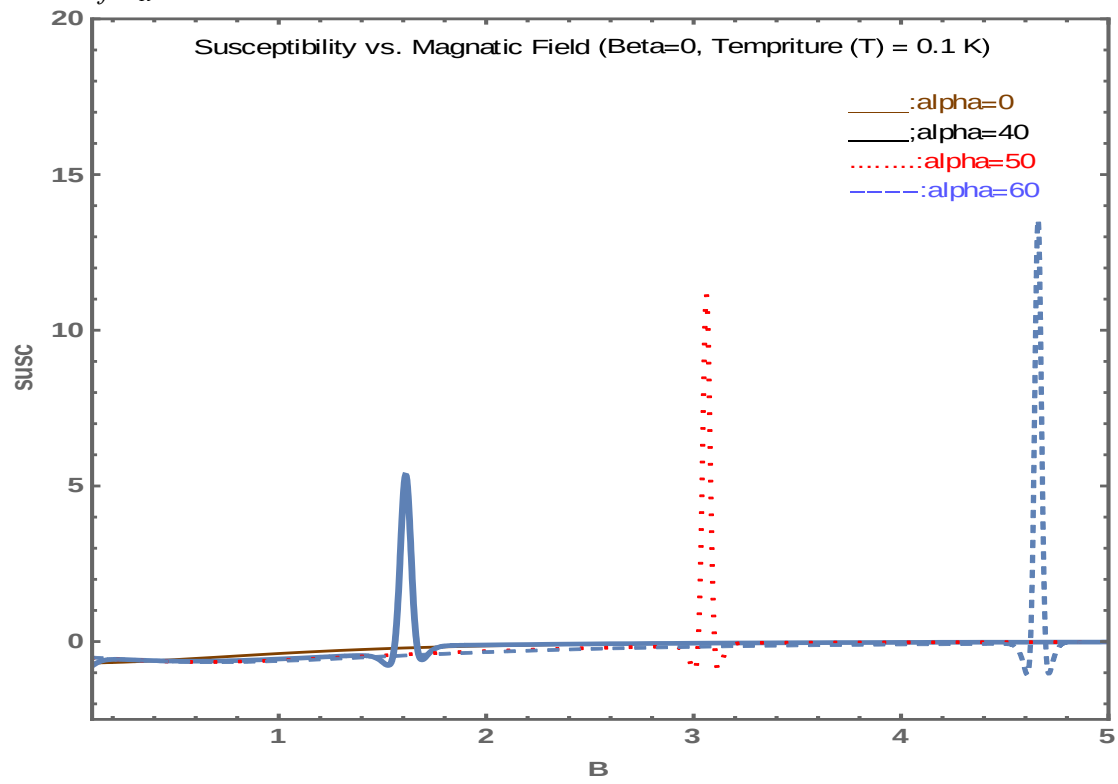

Figure 3.15

Susceptibility (χ) Vs. B(T) at T=10K and β_D =0 meV nm at five different values of α_R

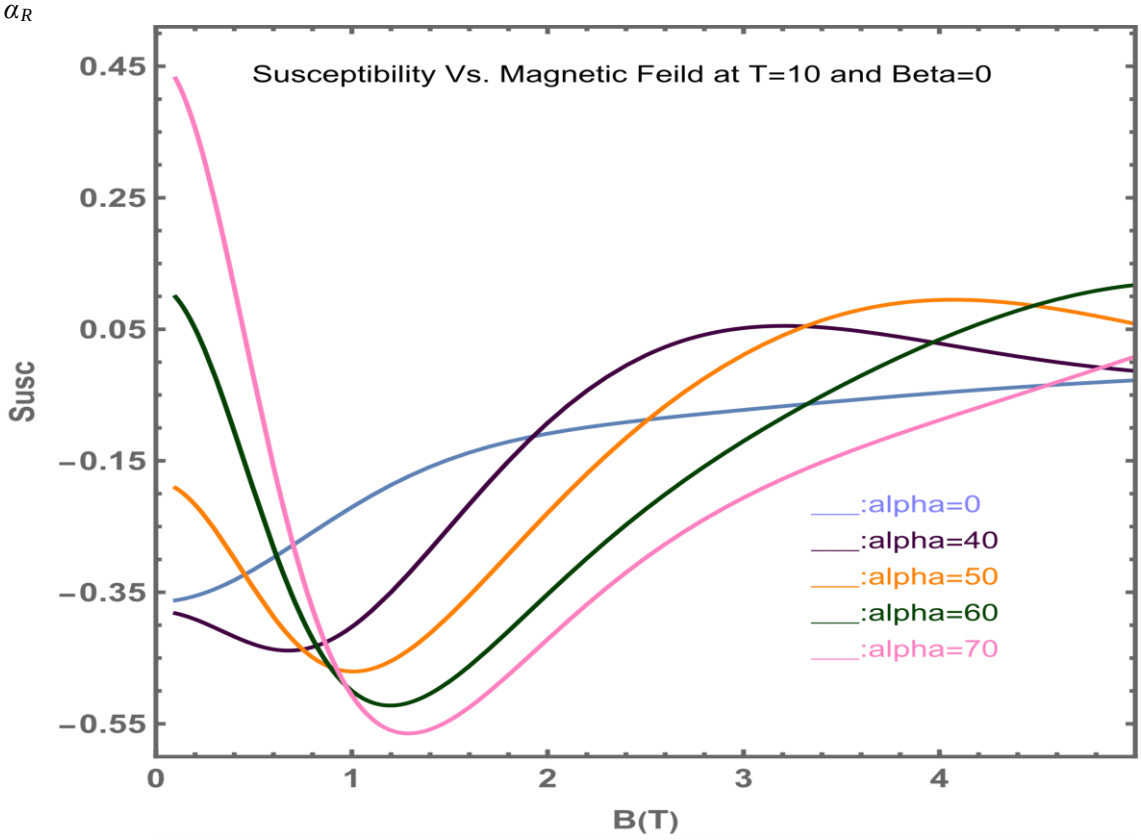

Figure 3.16

Susceptibility Vs. B(T) at T=0.1K, and five different values of αR and βD

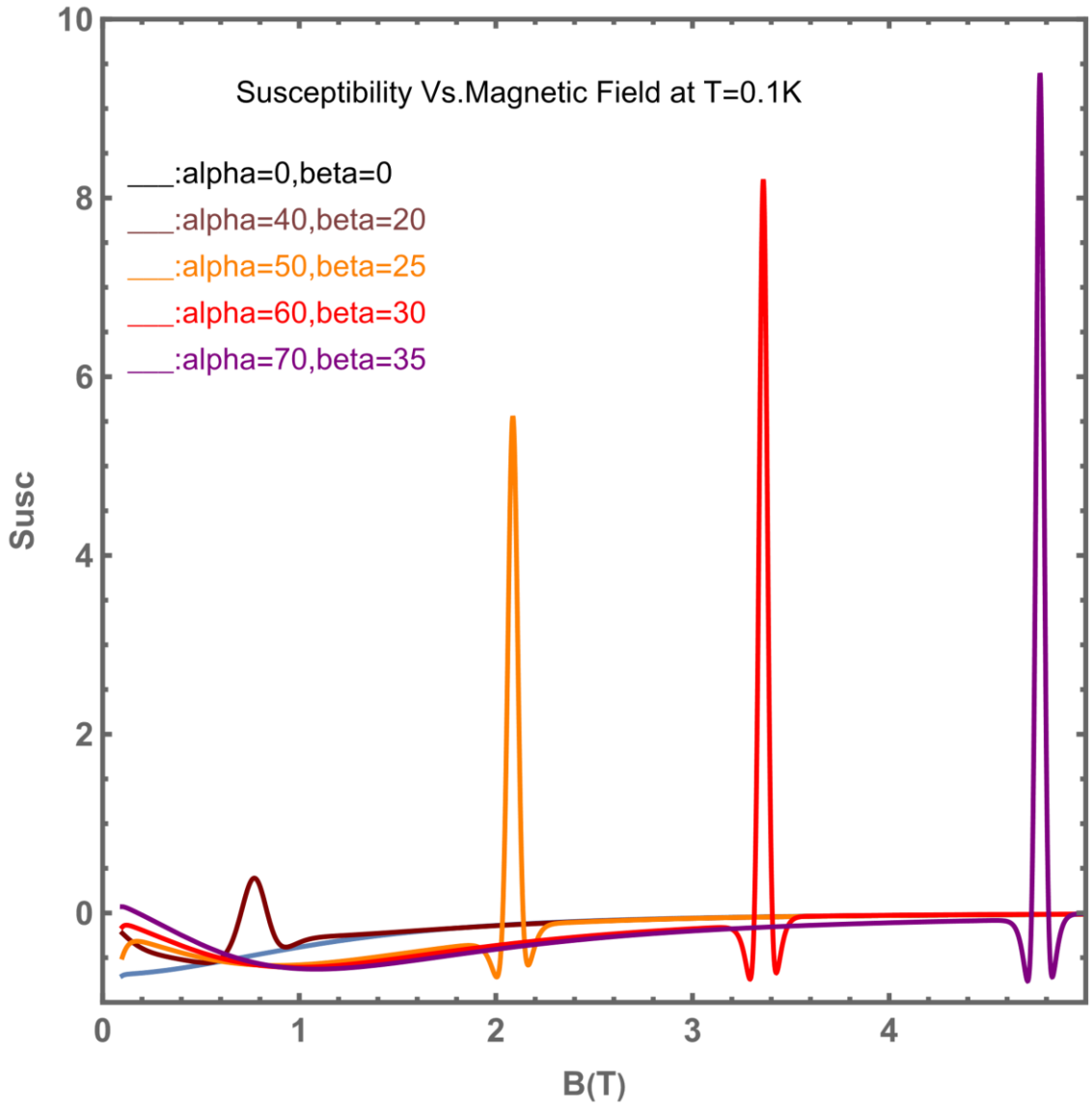

Figure 3.17

Susceptibility against. the magnetic field at T =10K and different values of α_R *and* $\beta_D = \frac{\alpha R}{2}$.

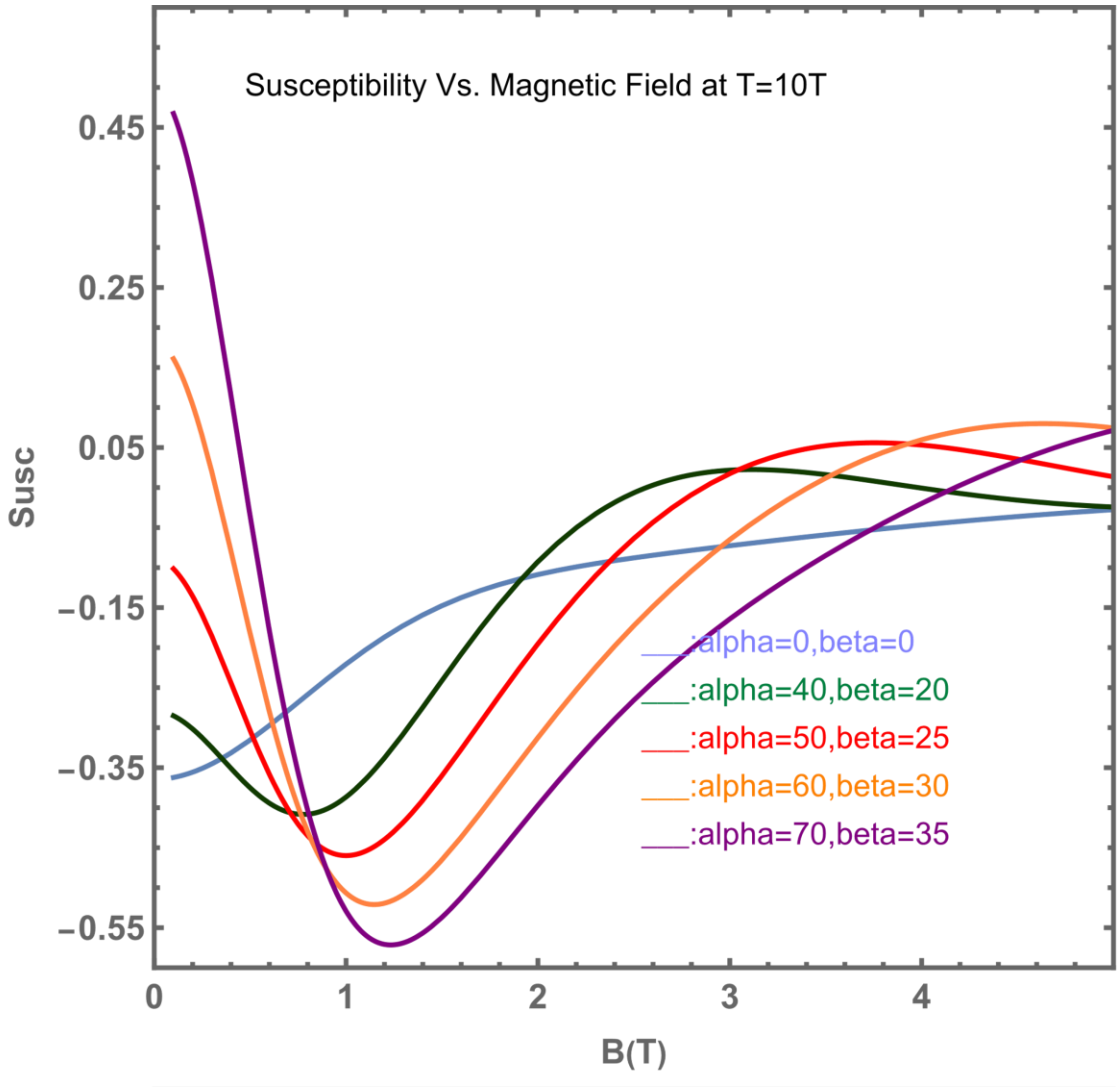

Figure 3.18

Plot of average energy as a function of B at $\boldsymbol{\gamma}$ *= 1 and 4 at (a) T=0.1K and (b)T=10K*

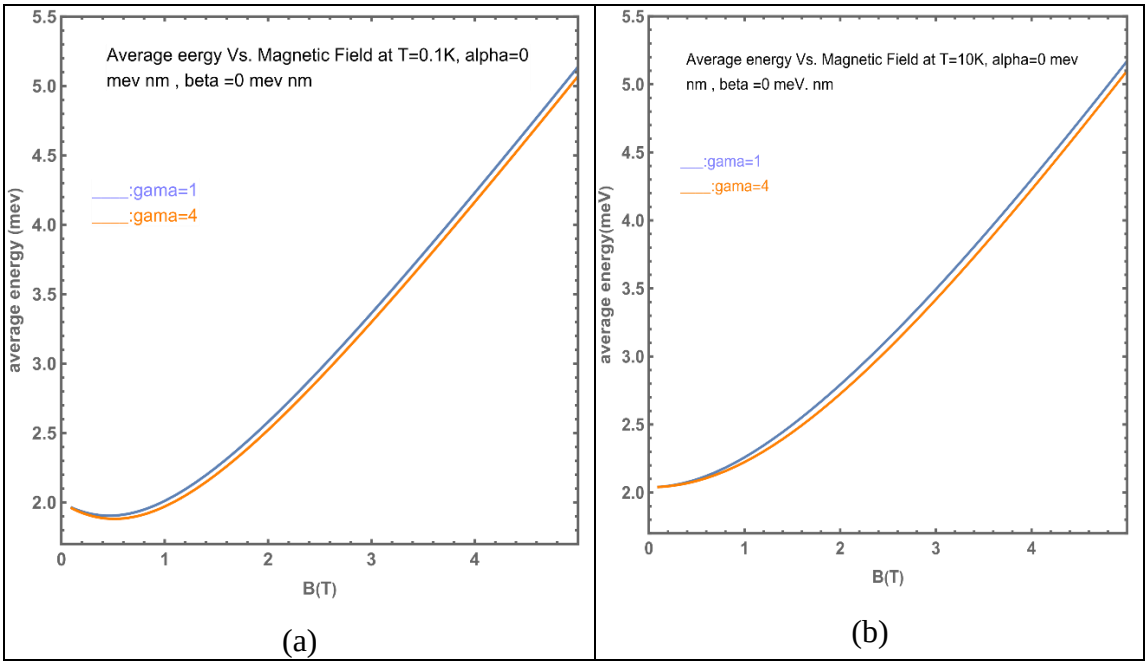

Figure 3.19

*a plot of average energy (****meV****) as a function of B(T) under Rashba, Dresslhaus and Tarnseverese effects with* α_R *=40 meV nm and* β_D *=20 meV nm and two veluse of* $\boldsymbol{\gamma}$ *=* **1 *and* 4 *meV*.*nm*** *(a) T =0.1K and (b) T =10K.*

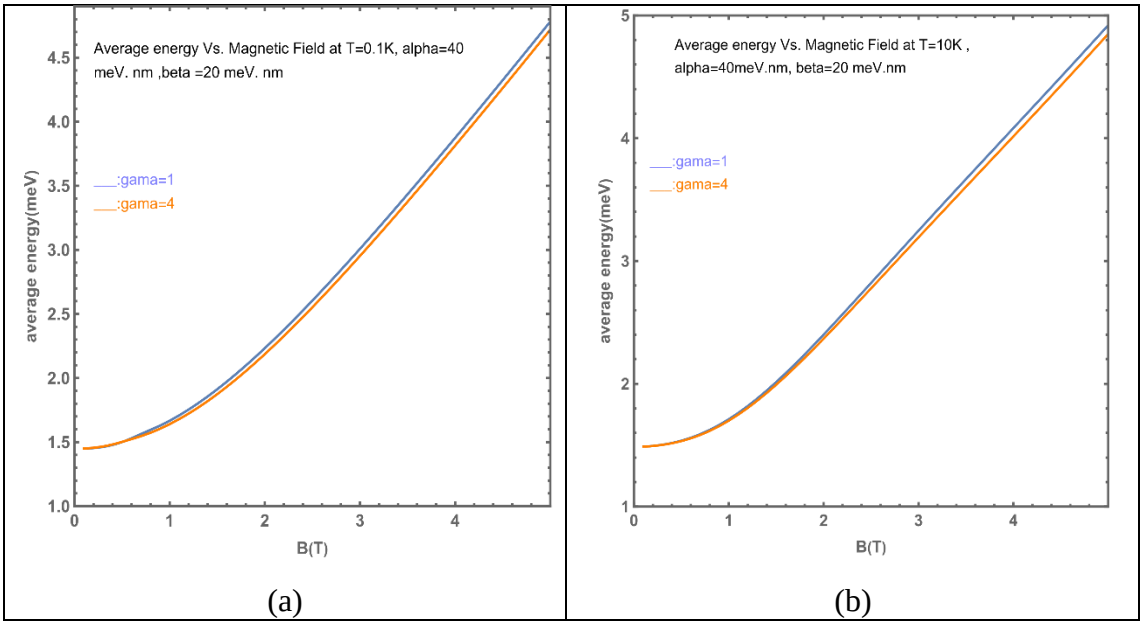

Figure 3.20

Plot of Magnetization $\boldsymbol{M}$ *as a function of B at* $\boldsymbol{\gamma = 1 \,\&\, 4\ meV.nm}$ *under (a) T=0.1K (b) T =10K*

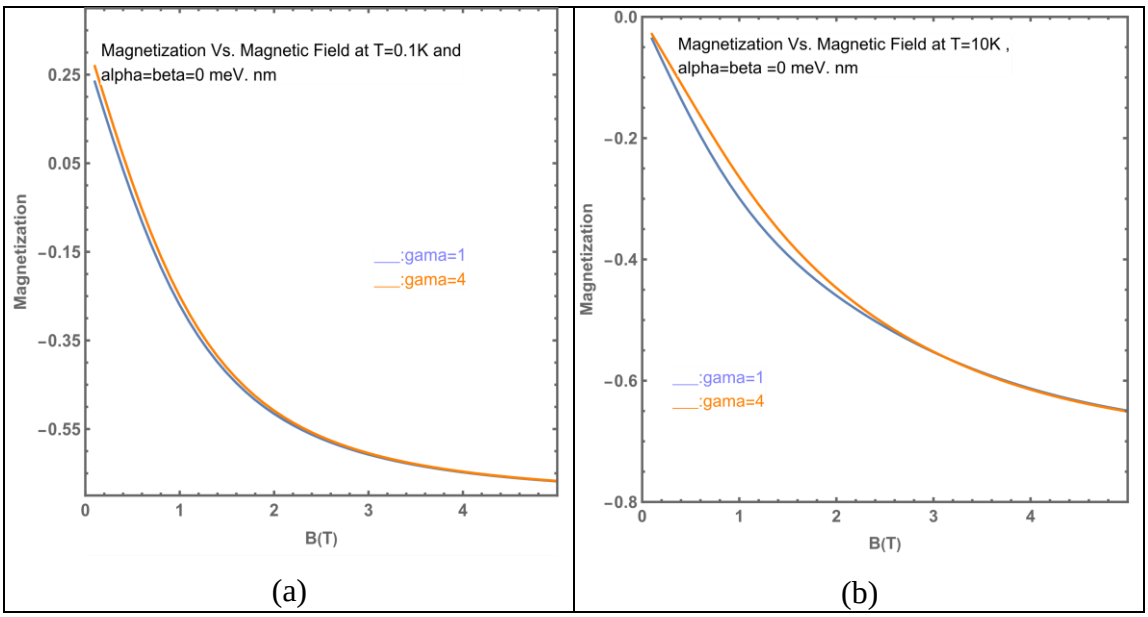

Figure 3.21

a plot of Magnetization as a function of B (T) with α_R*=40 meV. nm,* β_D*=20 meV. nm and* $\boldsymbol{\gamma = 1,4\ meV.nm}$ *at: (a) low T=0.1 K, (b) high T=10 k.*

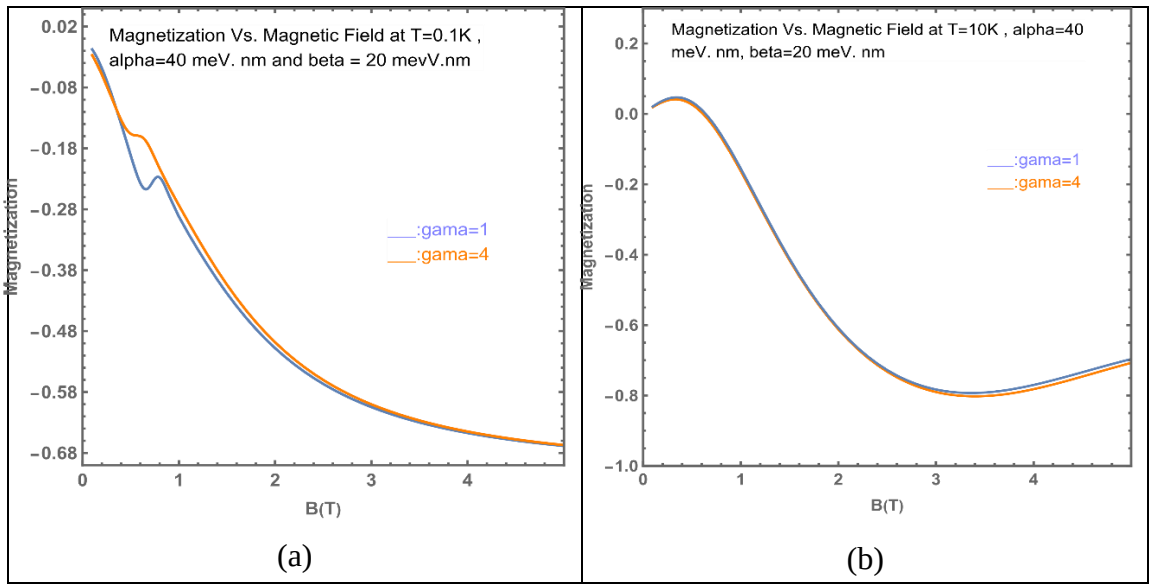

Figure 3.22

a plot of susceptibility as a function of B(T) at T=0.1 K and $\boldsymbol{\gamma = 1, 4\ meV.nm}$.

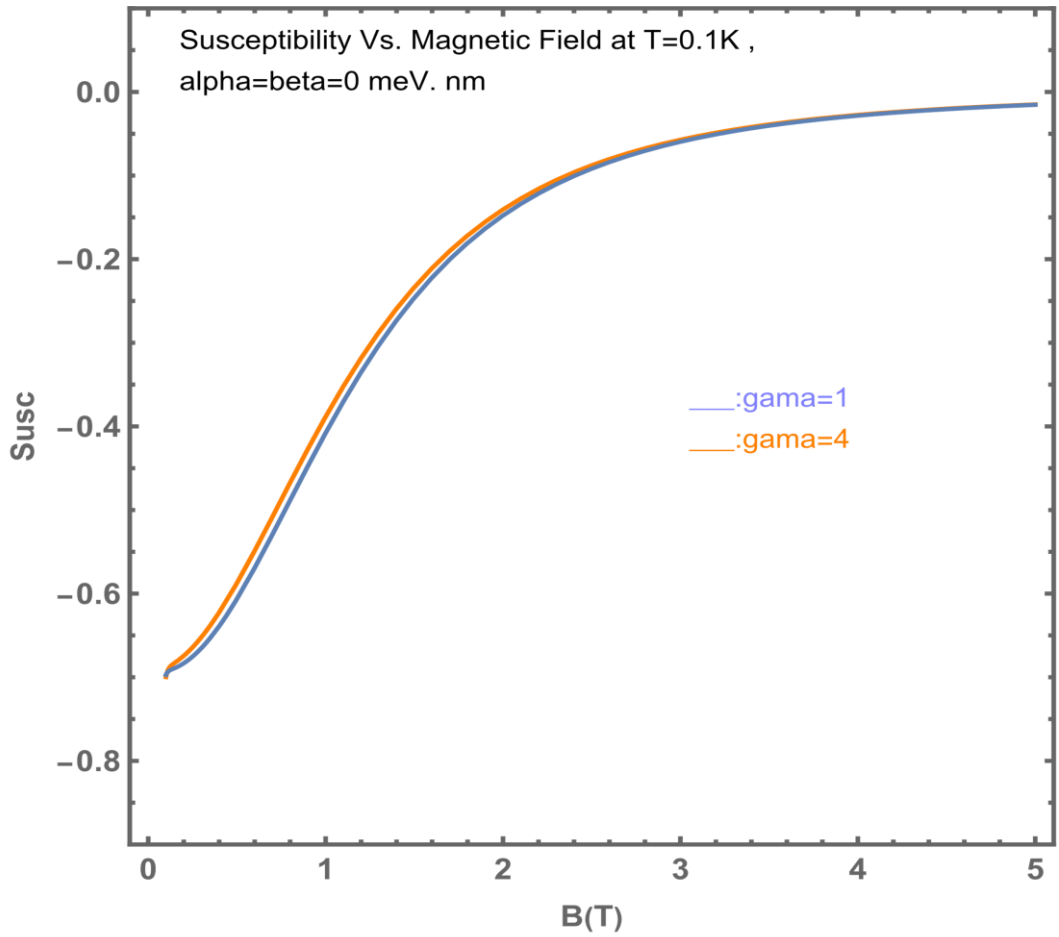

Figure 3.23

a plot of susceptibility as a function of B(T) at $\boldsymbol{\gamma = 1\ and\ 4\ meV.nm}$ α_R *= 40 meV. nm,* β_D *= 20meV. nm at (a) T=0.1K and (b) T=10K.*

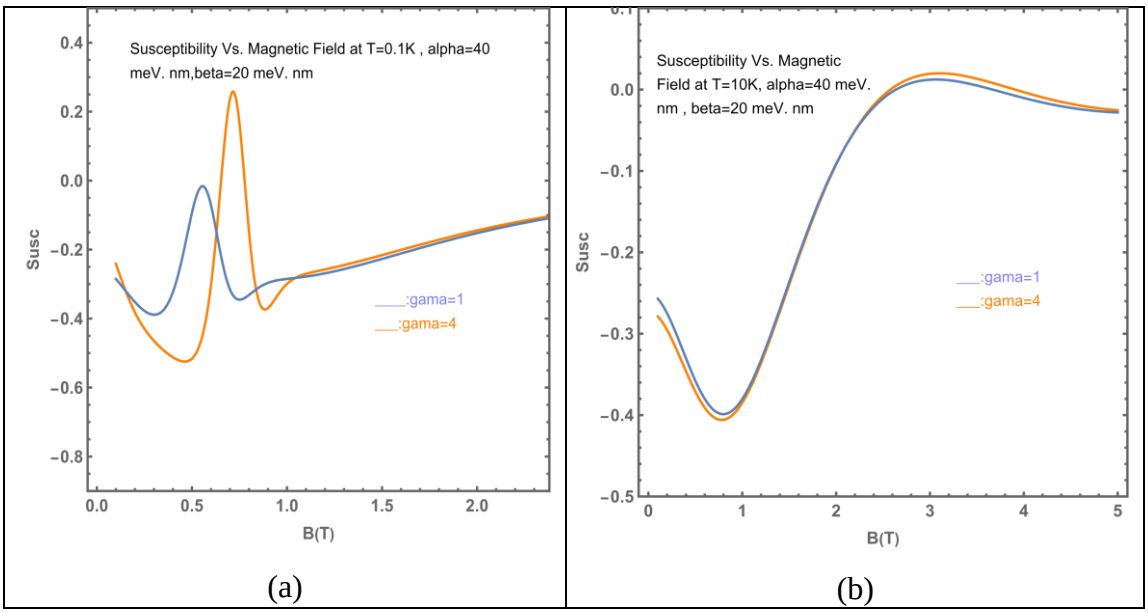

(a) (b)

جامعة النجاح الوطنية
كلية الدراسات العليا

تأثيرات ظاهرتي "رشبا" و"دريسلهوس" على القابلية المغناطيسية والمغنطة لسلك نانوي من مادة InAs

إعداد
وفاء أسامة حج محمد

إشراف
أ. د. محمد السعيد
د. معن اشتيوي

قدمت هذه الأطروحة استكمالاً لمتطلبات الحصول على درجة الماجستير في الفيزياء بكلية الدراسات العليا في جامعة النجاح الوطنية في نابلس –فلسطين.
2022

تأثيرات ظاهرتي "رشبا" و"دريسلهوس" على القابلية المغناطيسية والمغنطة لسلك نانوي من مادة InAs

إعداد

وفاء أسامة حج محمد

إشراف

أ. د. محمد السعيد

د. معن اشتيوي

الملخص

خلفية الدراسة: تلعب المواد النانوية دورًا مهمًا نظرًا لإمكانياتها في مجموعة واسعة من التطبيقات. يتم تصنيف المواد النانوية إلى أربعة أنواع وفقًا للأبعاد وهذه الأنواع هي: الثلاثية الأبعاد، الثنائية الأبعاد أو البئر الكمي (QW)، الأحادية الأبعاد أو سلك الآبار الكمومية (QWW) والنقطة الكمية أي صفرية الأبعاد (QD) . قامت العديد من الأبحاث بدراسة خصائص InAs QW و QWW في وجود المجال الكهربائي. في هذه الأطروحة تمت دراسة الخواص المغناطيسية لمادة InAS QWW تحت تأثيري راشبا ودريسيلهوس وتأثيرات المجال المغناطيسي. تم أخذ إمكانات الحبس المستعرض في الاعتبار أيضًا.

منهجية الدراسة: قمنا بدراسة تأثير المجال المغناطيسي على الخصائص المغناطيسية مثل التمغنط والقابلية المغناطيسية لسلك نانوي مصنوع من InAs تحت تأثير ظاهرتي رشبا ودريسلهوس عن طريق حل دالة هاملتون لحساب مستويات الطاقة لهذا السلك النانوي بدلالة متغيرات فيزيائية باستخدام حساب قطرية المصفوفة. تأثير المتغيرات الفيزيائية مثل: شدة المجال المغناطيسي، تردد الحصر، تأثير رشبا، تأثير دريسلهوس ودرجة الحرارة بدا واضحا على كل من: مستويات الطاقة ومعدل الطاقة وعلى الخواص المغناطيسية (التمغنط والقابلية المغناطيسية) لهذا السلك النانوي. ثم قمنا بدراسة تأثير ظاهرة إمكانات الحبس وشدة المجال المغناطيسي على معدل الطاقة والتمغنط والقابلية المغناطيسية أولا وبدا تأثير إمكانات الحبس ضعيفاً جداً مقارنةً بتأثيري رشبا ودريسلهوس، ثم بعد ذلك أضفنا كل من المتغيرات الفيزيائية: تأثير إمكانات الحبس، شدة المجال المغناطيسي، تأثير رشبا، تأثير دريسلهوس ودرجة الحرارة على كلٍ من معدل الطاقة

وعلى الخواص المغناطيسية مجدداً وأوضحت النتائج أن تأثير إمكانات الحبس مع تأثيري رشبا ودريسلهوس كان أوضح من وجود تأثير إمكانات الحبس وحده.

أثبتت **النتائج** الحسابية جلياً أن تأثير رشبا على الخصائص المغناطيسية كان قوياً ومهما وأكثر وضوحاً من تأثير دريسلهوس للتحكم بالتمغنط والقابلية المغناطيسية لهذا السلك النانوي المصنوع من مادة InAs وكان تأثير إمكانات الحبس ضعيفاً جدا مقارنةً بتأثيري رشبا ودريسلهوس ولكن تأثيره موجود.

الاستنتاجات: إن تأثير رشبا كان عاملاً فعالاً ومهماً للتحكم في الخصائص المغناطيسية لمادة InAs QWW. وتأثير دريسلهوس يتحكم أيضاً في الخصائص المغناطيسية للمادة ولكن بشكل أضعف من تأثير رشبا. إن إمكانات الحبس لها تأثر هامشي وضعيف جداً على كل من المغنطة والقابلية المغناطيسية للمادة.

الكلمات المفتاحية: تأثير رشبا، تأثير دريسلهوس، *InAs QWW*، المجال المغناطيسي، المغنطة، القابلية المغناطيسية.